Available online at www.sciencedirect.com
SCIENCE DIRECT®
Precambrian Research 124 (2003) 107–148
Precambrian Research
www.elsevier.com/locate/precamres

Derivation of the 1.0–0.9 Ga ferro-potassic A-type granitoids of southern Norway by extreme differentiation from basic magmas

Jacqueline Vander Auwera [a,*], Michel Bogaerts [a,1], Jean-Paul Liégeois [b], Daniel Demaiffe [c], Edith Wilmart [a,d], Olivier Bolle [a], Jean Clair Duchesne [a]

[a] *L.A. Géologie-Pétrologie-Géochimie (B20), Université de Liège, B-4000 Sart Tilman, Belgium*
[b] *Section de Géologie Isotopique, Africa Museum, B-3080 Tervuren, Belgium*
[c] *Département des Sciences de la Terre (CP160/02), Université Libre de Bruxelles, B-1050 Bruxelles, Belgium*
[d] *CETP, 10/12 Avenue de l'Europe, 78140 Vélizy, France*

Received 10 October 2001; received in revised form 28 September 2002

Abstract

Major and trace elements, Sr and Nd isotopic data as well as mineral compositions are presented for a selection of the 1.0–0.9 ferro-potassic A-type granitoids (Bessefjellet, Rustfjellet, Verhuskjerringi, Valle, Holum, Svöfjell, Handeland-Tveit, Åseral, Lyngdal gabbronorites) that occur close to the Mandal-Ustaoset Line (MUL) of southern Norway. These hornblende biotite granitoids (HBG) define an extensive differentiation trend ranging from gabbronorites (50 wt.% SiO_2) to granites (77 wt.% SiO_2). This trend is interpreted as resulting from extreme fractional crystallization of several basaltic magma batches with similar major and trace elements compositions. At 930 Ma, the HBG suite displays a narrower range in I_{Sr} (0.7027–0.7056) than in $\varepsilon_{Nd(t)}$ (+1.97 down to −4.90) suggesting some assimilation of a Rb-depleted lower crust (AFC process) or/and source variability. An age of 929 ± 47 Ma is given by a Rb-Sr isochron on the Holum granite ($Sr_i = 0.7046 \pm 0.0006$, MSWD = 1.7). Geothermobarometers indicate a low pressure of emplacement (1.3–2.7 kbar) and an oxygen fugacity close to NNO. High liquidus temperatures are given by the apatite saturation thermometer (1005–1054 °C) and are in agreement with results from other studies. The basaltic parent magmas of the HBG suite are partial melts of an hydrous mafic, potassic source lying either in the lithospheric upper mantle or in the mafic lower crust derived from it. This contrasts with the 930 Ma anorthosite–mangerite–charnockite suite (AMC suite) of the Rogaland Province for which a depleted lower crustal anhydrous gabbronoritic source has been indicated. The present data imply the penecontemporaneous melting of two contrasting sources in southern Norway. The source duality could result from an increasing degree of metamorphism (amphibolite to granulite) from East to West, an horizontal stratification of the lower crust or from the stratification of the lithosphere (melting of the lower crust or upper mantle). It may also indicate that the AMC and HBG suites formed in two distinct crustal segments. The linear alignment of the HBG suite along the Mandal-Ustaoset shear zone suggests that a linear uprise of the asthenosphere, following a lithospheric delamination under this structure, could be the vector of the mantle heat.

Keywords: A-type; Granites; Sveconorwegian; Proterozoic; Southern Norway

1. Introduction

At about 1.0–0.9 Ga, the southwestern Baltic shield (southern Norway and Sweden) was intruded by a

* Corresponding author. Tel.: +32-4-3662253; fax: +32-4-3662921.
E-mail address: jvdauwera@ulg.ac.be (J.V. Auwera).
[1] Aspirant du Fonds National Belge de la Recherche Scientifique.

0301-9268/03/$ – see front matter © 2003 Elsevier Science B.V. All rights reserved.
doi:10.1016/S0301-9268(03)00084-6

suite of late granitoids related to the main Sveconorwegian deformation structures (Andersson et al., 1996). Considerable volume of magma was emplaced in a short time (Fig. 1) creating a large scale phenomenon affecting the Proterozoic continental crust. These late granitoids belong to the distinctive rock type, usually referred to as A-type, occurring in most Proterozoic belts. The origin of this granitoid suite is

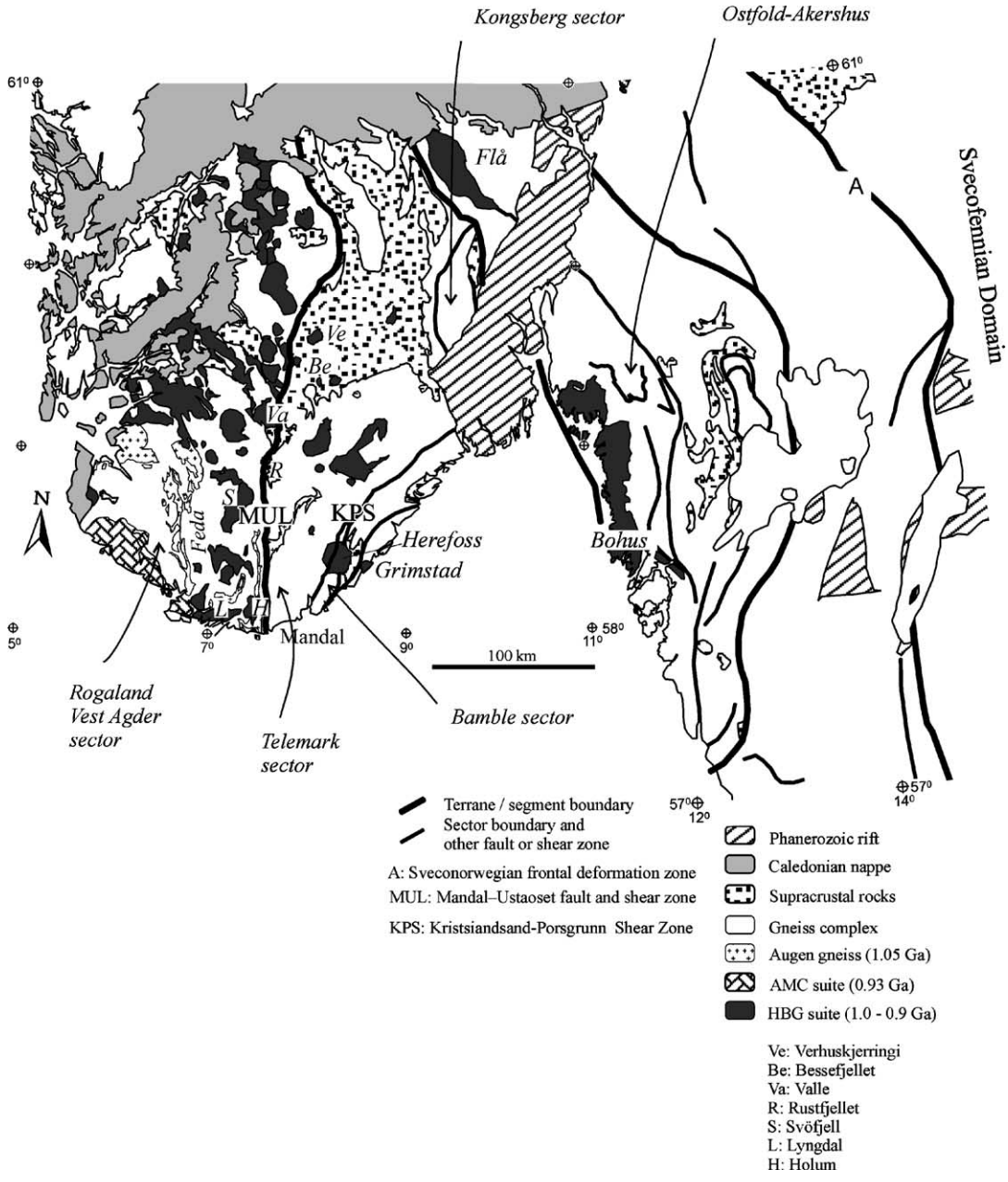

Fig. 1. Sketch map of the Sveconorwegian Province from Bingen et al. (2001). The Åseral and Handeland-Tveit intrusions located south of the Svöfjell massif as well as the Lyngdal gabbronorites emplaced just north of the Lyngdal granodiorite are not shown in the figure because of their small size.

currently under considerable debate. Geochronological and isotopic data already exist for some of the Sveconorwegian granitoids (Andersen et al., 2001). They indicate similar ages between 1.0 and 0.9 Ga (see Andersson et al., 1996 for a summary of available geochronological data) and the Nd, Sr and Pb systematics suggest mixing between a depleted mantle component and two or more components having an extended crustal history (Andersen et al., 2001). The purpose of this study is to examine the geochemistry (major and trace elements as well as Nd and Sr isotopes) and petrology of a selection of these granitoids outcropping in the Vest Agder and Telemark sectors of southern Norway, in order to define possible differentiation trends, the parent magma compositions as well as possible sources. Indeed, it has already been recognized that A-type Proterozoic granites encompass different granite compositions (metaluminous, peraluminous, peralkaline) which may have different sources (Poitrasson et al., 1995). On the other hand, in southern Norway as in many other Proterozoic belts, these granitoids are close in space and time with an anorthosite–mangerite–charnockite suite (AMC suite), the Rogaland anorthosite complex, for which a complete liquid line of descent has been defined (Demaiffe and Hertogen, 1981; Duchesne et al., 1974; Vander Auwera et al., 1998a; Wilmart et al., 1989) and a lower crustal gabbronoritic (mafic anhydrous) source has been indicated (Longhi et al., 1999). It is thus also important to constrain the source of the penecontemporaneous granitoid suite which is studied here in order to better characterize its relationship with the AMC suite and the overall evolution of this segment of the Proterozoic continental crust.

2. Geological outline

The Precambrian basement of southern Norway belongs to the southwest Scandinavian domain of the Baltic shield. It has been subdivided in five sectors (Rogaland-Vest Agder, Telemark, Bamble, Kongsberg, Ostfold-Akershus) separated by major crustal lineaments (Fig. 1). The first two, in which occur the intrusions discussed in this paper, are separated by the Mandal-Ustaoset Line (MUL) (Sigmond, 1985) that crops out as a brittle fault zone in its northern and central parts and as an elongated augen gneiss in its southern part. Similarly, the Feda augen gneiss which is also N-S elongated (Fig. 1) could delineate a major crustal structure (shear zone) separating the Rogaland anorthositic province to the West and the Vest Agder migmatitic province to the East (Duchesne et al., 1999). The Telemark sector is bounded to the East by the Kristiansand-Porsgrunn shear zone (KPS in Fig. 1).

The Telemark and Rogaland-Vest Agder sectors are made up of high grade gneisses (migmatites with a supracrustal protholith, granitic gneisses and augen gneisses) and low grade supracrustal formations (the Telemark Supergroup), intruded by pre-, syn- and postcollisional Sveconorwegian intrusions. Geochronological data obtained in these two sectors range from 1600 to 800 Ma and reveal a complex metamorphic and tectonic evolution (i.e. Jacobsen and Heier, 1978; Menuge, 1982; Pasteels and Michot, 1975; Priem and Verschure, 1982; Tobi et al., 1985). Classically, ages between 1.75 and 1.5 Ga have been related to the Gothian orogeny and those ranging from 1.2 to 0.9 Ga belong to the Sveconorwegian orogeny.

In the Rogaland-Vest Agder and Telemark sectors, magmatism occurred at various stages of the tectonic evolution. The Hidderskog (Zhou et al., 1995), Botnavatnet and Gloppurdi massifs (Wielens et al., 1981) were emplaced at about 1160 Ma, prior to the main Sveconorwegian event, and display an A-type signature (Zhou et al., 1995). The high-K calc-alkaline augen gneisses were emplaced at the climax of the orogeny around 1.05 Ga (Bingen et al., 1993). The postcollisional intrusions can be separated in two groups. One group corresponds to the Rogaland AMC suite, emplaced in a short period of time between 930 and 920 Ma in the western Rogaland-Vest Agder sector (Pasteels et al., 1979; Schärer et al., 1996). The second group comprises a series of biotite/hornblende-bearing granitoids (HBG suite) forming a ≈300 km long belt stretching along the MUL. It includes the Lyngdal granodiorite (Bogaerts et al., 2001; Bogaerts et al., in press; Falkum and Petersen, 1974; Falkum et al., 1972; Falkum et al., 1979; Petersen, 1980a,b). This HBG suite belongs to the voluminous 1.00–0.90 Ga postcollisional plutonism occurring in southern Norway and eastwards and represented, among others, by the Grimstad pluton in the Bamble sector, the Herefoss granite crosscutting the Kristiansand-Porsgrunn shear zone (Andersen, 1997:

Table 1
Sample location (*X–Y* coordinates in the EURF89 kilometric UTM grid) and description

Massif	Sample #	Locality	E EUREF89	N EUREF89	Description
Valle	VA1	Road 12	15.719	15.719	Porphyritic granodiorite
(Zone 32VML)	VA2	Road 12	15.719	62.443	Porphyritic granite
Verhuskjerringi	S1	S Öygarden	54.519	13.693	Granite
(Zone 32VMM)	S2	S Öygarden	54.519	13.693	Granite
	S6	Grönli	50.419	07.793	Granite
	S7	Close to Tjönnestöl	48.719	11.993	Aplite
	S8	Close to Tjönnestöl	48.719	11.993	Leucogranite
Bessefjellet	BE1-90A	Road 38 to Dalen	41.419	95.593	Granite
(Zone 32VML)	BE1-90D	Road 38 to Dalen	41.419	95.593	Granite
	BE3	Road 38 to Dalen	41.419	95.593	Leucogranite
	BE4	Storehaug	37.819	99.093	Leucogranite
	BE5	Skuggenut	37.919	98.443	Leucogranite
	BE6	Vidsynnut	38.019	98.143	Leucogranite
	BE90-1A	E Tjönnstöl	37.269	94.793	Leucogranite
	BE90-1B	E Tjönnstöl	37.269	94.793	Leucogranite
	BE90-2	SW to point 1081 m	38.219	95.693	Leucogranite
	BE90-3	Point 1081 m	38.469	95.893	Leucogranite
	BE90-4	E Svartetj	38.569	96.693	Aplite
	BE90-5	E Svartetj	38.119	96.493	Leucogranite
Holum	98BN2A	NW Hennestad	07.240	51.850	Granite
(Zone 32VMK)	98BN6	W Kalland	11.360	39.310	Granite
	98BN9B	E Hålandsheia	09.450	35.630	Granite
	98BN25C	N Solås	10.360	44.740	Granite
	98BN33C	Erland	06.530	43.540	Porphyroidic granite
	98BN39A	NE Norum	08.780	43.390	Granite
	98BN39B	id.	08.780	43.390	Granite
	98BN41C	Birkeland	06.040	42.250	Granite
	98BN44C	W Holum	11.330	40.760	Porphyroidic granite
	98BN46C	Ljosevatnet	09.180	40.550	Porphyroidic granite
	98BN50C	E Møglandsheia	06.710	39.730	Porphyroidic granite
	98BN58C	Spetteland	08.990	37.780	Granite
	98BN65C	NE Mjåvatnet	11.480	42.900	Granite
	98BN72D	E Flagmyråsen	09.930	51.150	Granite
	98BN81C	SE Drøpta	05.600	45.540	Granite
	98BN90C	Homestad	09.200	52.360	Porphyroidic granite
	98BN93C	Høylandsvatnet	10.700	47.780	Porphyroidic granite
	98BN99D	NE Ljosstøl	07.360	49.800	Porphyroidic granite
	98BN100C	Tjomsland	06.390	48.350	Granite
Holum/inclusions	98BN11	NE Løkke	08.660	36.550	Granite
(granitic gneiss ?)	98BN21E	W Kvitbergsskor	11.560	44.660	Leucogranite
(Zone 32VMK)	98BN31C	W Kartemyrheia	08.260	45.610	Granite
	98BN73C	S Jogelstjørna	09.030	48.630	Granite
Handeland-Tveit	HA1	Skareberglia	11.289	92.193	Quartz diorite
(Zone 32VMK)	H7	Nesland	10.269	92.293	Quartz diorite
	H12	Skareberglia	11.219	92.293	Quartz diorite
	H14	Nesland	10.319	92.343	Quartz monzodiorite
	H18	Handeland	11.069	92.593	Quartz diorite
	H22	Handeland	10.819	92.493	Quartz diorite
Svöfjell	84-43	S Ljosland	07.319	09.693	Granite
(Zone 32VML	84-44	Kvernevatnet	02.619	18.093	Granite
except when noted)	84-47	Kvernevatnet	02.619	18.093	Aplite
Zone 32VLL	84-52	Kvernevatnet	99.669	18.713	Granite
Zone 32VLL	84-53	Kvernevatnet	99.669	18.713	Granite

Table 1 (*Continued*)

Massif	Sample #	Locality	E EUREF89	N EUREF89	Description
	84-62	Svartevatn	04.819	04.993	Granite
	84-64	Svartevatn	04.819	04.993	Aplite
	84-66	S Ljosland	05.069	15.693	Granite
	SV1	Langevatn	06.419	21.793	Granite
	SV2	Langevatn	05.719	20.143	Granite
	SV3	N Ljosland	05.819	18.993	Granite
	SV4	Ljosland	05.069	18.193	Granodiorite
	SV5	S Ljosland	04.969	16.793	Granodiorite
	SV6	S Ljosland	05.169	15.893	Granodiorite
	SV7	S Ljosland	05.219	15.043	Granite
	SV8	S Ljosland	05.619	14.493	Granite
	SV9	S Ljosland	06.619	12.593	Granite
	SV10	S Ljosland	06.669	11.693	Granite
	SV11	S Ljosland	06.969	10.493	Granite
	SV12	S Ljosland	07.219	08.693	Granodiorite
Zone 32VLL	SV13	Knaberöysi	94.419	05.043	Granodiorite
	SV90-10	W Ljosland	04.119	17.893	Granite
	SV90-12	N Ljosland	04.519	17.993	Granite
	SV90-13	Ljosland	05.019	17.693	Quartz monzodiorite
	SV90-14	E Farvatn	03.419	17.193	Granite
Svöfjell/dykes	84-48	Kvernevatnet	01.519	17.993	Leucocharnockite
(Zone 32VML)	84-50	Kvernevatnet	01.519	17.993	Leucocharnockite
	84-59	E Seldal	06.119	04.593	Charno-enderbite
	SV90-6	Seldal	06.369	04.643	Leucocharnockite
	SV90-8	Kvernevatnet	02.669	18.393	Leucocharnockite
Rustfjellet	R2	Rustfjell	19.119	35.743	Leucogranite
(Zone 32VML)	R3	Rustfjell	19.119	35.743	Leucogranite
	R5	Rustfjell	18.519	35.393	Leucogranite
	R6	Rustfjell	18.119	35.643	Leucogranite
	R7	Rustfjell	18.919	36.893	Leucogranite
	R8	Rustfjell, point 1059 m	18.269	35.193	Granite
	R10	Rustfjell, point 1059 m	18.269	35.193	Granite
	R11	Rustfjell, point 1053 m	18.419	34.593	Leucogranite
	R12	Rustfjell	19.169	34.593	Leucogranite
Aseral	A1	Road to Grönli	07.119	99.043	Quartz monzodiorite
(Zone 32VMK)	A5	Aseral	07.669	98.493	Quartz monzodiorite
	A10	Öyard	06.539	99.793	Quartz monzodiorite
Gneisses	VDA 9902	Skjeggestad	55.359	85.013	Leucogabbronoritic gneiss
(Zone 32VLK)	VDA 9905	Tjörnhom	78.969	76.043	Amphibolitic gneiss
	VDA 9906	Tjörnhom	78.969	76.043	Charnockitic gneiss
	VDA 9907	Tjörnhom	78.969	76.043	Banded gneiss
	VDA 9903C	Skjeggestad	55.359	85.013	Charnockitic gneiss
	VDA 9903F	Skjeggestad	55.359	85.013	Charnockitic gneiss
	VDA 9904	Skjeggestad	55.359	85.013	Banded gneiss

926 ± 8 Ma, $Sr_i = 0.7046$; $\varepsilon_{Nd} = -3.2$ to -0.8) and the Bohus-Flå granite belt stretching for at least 300 km from northern Telemark down to the west coast of Sweden along several large scale tectonic lineaments (Andersen et al., 2001; Andersson et al., 1996) (Fig. 1). Recently, Andersen et al. (2001) have suggested that most of the granites occurring all over southern Norway, result from the mixing between a depleted mantle-derived component and two or more major components having a long crustal history.

We present here a petrological study of eight intrusions (90 samples) selected among the granitoids related to the MUL. These intrusions are from North to South Verhuskjerringi, Bessefjellet, Valle, Rustfjellet,

Svöfjell, Åseral (not shown), Handeland-Tveit (not shown) and Holum (Fig. 1). The following discussion will also include the undeformed Lyngdal hyperites (gabbronorites to monzonorites) cropping out as two small intrusions north of the Lyngdal granodiorite and studied by Demaiffe et al. (1990). The intrusions are shown in Fig. 1 and the *X*–*Y* coordinates of samples are given in Table 1. A detailed geochemical and experimental study of the Lyngdal granodiorite is in progress (Bogaerts et al., 2001; Bogaerts et al., in press).

3. Analytical methods

Microprobe analyses of feldspars, amphiboles, biotites, Fe-Ti oxides and clinopyroxenes have been performed with the Cameca SX50 of the CAMST ("Centre d'analyses pour les Sciences de la Terre", Louvain-La-Neuve, Belgium) on selected samples of the granitoids. Accelerating voltage was set at 15 kV and elements were counted for 20 s (Ca, K, Ti, Cl), 30 s (Si, Al, Fe, Mg, Mn, Cr) or 45 s (Na, F) at a beam current of 20 nA. A combination of synthetic and natural standards were used and X-ray intensities were reduced using the Cameca PAP correction program. Results are shown in Tables 2–5.

Ninety whole-rock samples were selected for a geochemical study. Major and some trace elements were analyzed by X-ray fluorescence (ARL 9400 XP for Holum samples and CGR ALPHA 2020 for all other samples) following the method described in Bologne and Duchesne (1991) for samples analyzed with the CGR ALPHA 2020. Other trace elements including rare earths were analyzed with the ICP-MS (VG Plasma Quad PQ2) following the method described in Vander Auwera et al. (1998b) or/and INAA (Pierre Süe Laboratory: CEA, Saclay, France). FeO was measured by titration. Results are shown in Table 6.

Sr and Nd isotopes were measured on a selection of samples. Results are shown in Table 7. After acid dissolution of the sample and Sr and Nd separation on ion-exchange resin, Sr isotopic compositions have been measured on Ta simple filament and Nd isotopic compositions on triple Ta-Re-Ta filament on a Micromass Sector 54. Repeated measurements of Sr and Nd standards have shown that between-run error is better than ±0.000015. Within-run errors are generally lower. The NBS987 standard has given a value for $^{87}Sr/^{86}Sr$ of 0.710274 ± 0.000011 (2σ on the mean, four measurements, normalized to $^{86}Sr/^{88}Sr = 0.1194$) and the Rennes Nd standard (Chauvel and Blichert-Toft, 2001), a value for $^{143}Nd/^{144}Nd$ of

Table 2
Selected electron microprobe analyses of feldspars

	Rustfellet		Svöfjell			Verhuskjerringi			Valle		Bessefjellet	
	R7	R7	SV6	SV90-13	SV90-13	S2	S2	S2	VA1	VA1	BE1	BE1
SiO_2	65.33	65.24	62.36	65.22	61.17	65.73	64.05	61.31	64.59	63.23	65.53	65.54
Al_2O_3	18.45	22.16	24.42	18.43	24.73	18.65	23.11	24.66	18.41	23.65	18.31	22.08
FeO	0.00	0.00	0.10	0.00	0.11	0.22	0.23	0.30	0.07	0.04	0.00	0.16
CaO	0.04	3.56	6.29	0.04	6.68	0.16	4.71	6.59	0.00	5.25	0.00	3.20
Na_2O	0.80	9.81	8.15	1.43	7.88	2.38	9.07	7.83	0.88	8.84	0.56	9.90
K_2O	16.29	0.24	0.28	15.16	0.27	13.79	0.24	0.32	16.03	0.15	16.71	0.31
Total	100.91	101.01	101.60	100.28	100.84	100.93	101.41	101.01	99.98	101.16	101.11	101.19
Normalized to eight oxygens												
Si	2.995	2.850	2.729	2.996	2.702	2.990	2.798	2.705	2.989	2.770	3.001	2.858
Al	0.997	1.141	1.260	0.998	1.287	1.000	1.190	1.282	1.004	1.221	0.988	1.135
Fe^{2+}	0.000	0.000	0.004	0.000	0.004	0.008	0.008	0.011	0.003	0.002	0.000	0.006
Ca	0.002	0.167	0.295	0.002	0.316	0.008	0.220	0.311	0.000	0.246	0.000	0.150
Na	0.071	0.831	0.691	0.127	0.675	0.210	0.768	0.669	0.079	0.751	0.049	0.837
K	0.953	0.013	0.016	0.888	0.015	0.800	0.013	0.018	0.946	0.008	0.976	0.017
Ab	6.94	82.21	68.99	12.52	67.06	20.65	76.66	67.04	7.69	74.67	4.82	83.39
An	0.21	16.47	29.44	0.20	31.43	0.75	22.00	31.18	0.00	24.52	0.00	14.90
Or	92.86	1.32	1.57	87.29	1.51	78.60	1.34	1.79	92.31	0.81	95.18	1.71

Table 3
Selected electron microprobe analyses of amphiboles

	Svöfjell		Verhuskjerringi	Valle
	SV6	SV90-13	S2	VA1
SiO_2	43.68	43.68	45.27	42.08
TiO_2	0.95	1.24	1.72	0.42
Al_2O_3	9.08	9.39	8.03	10.21
Fe_2O_3	5.49	4.66	3.25	6.62
FeO	15.45	14.83	11.90	15.65
MnO	0.68	0.58	0.60	0.73
MgO	9.32	9.95	13.00	8.67
CaO	11.69	11.76	11.80	11.66
Na_2O	1.43	1.46	1.87	1.74
K_2O	1.42	1.47	1.50	1.72
Cr_2O_3	0.00	0.00	0.00	0.00
F	0.67	0.65	1.00	1.04
Cl	0.15	0.12	0.09	0.21
H_2O	1.64	1.67	1.54	1.44
Total	101.65	101.45	101.58	102.18
–O=F + Cl	0.32	0.30	0.44	0.49
Total	101.34	101.15	101.13	101.70
Normalized to 13 cations				
Si	6.556	6.534	6.664	6.358
Ti	0.107	0.139	0.190	0.048
Al	1.607	1.656	1.394	1.819
Fe^{3+}	0.620	0.524	0.361	0.752
Fe^{2+}	1.940	1.855	1.465	1.977
Mn	0.086	0.073	0.075	0.093
Mg	2.085	2.218	2.852	1.952
Ca	1.880	1.885	1.861	1.888
Na	0.416	0.423	0.534	0.510
K	0.272	0.281	0.282	0.332
Cr	0.000	0.000	0.000	0.000
F	0.318	0.307	0.466	0.497
Cl	0.038	0.030	0.022	0.054
OH	1.644	1.662	1.512	1.449
$Mg/(Mg + Fe^{2+})$	0.518	0.545	0.661	0.497

0.511956 ± 0.000012 (2σ on the mean, eight measurements, normalized to $^{146}Nd/^{144}Nd = 0.7219$) during the days of measurements. All measured ratios have been recalculated to the recommended values of 0.71025 for NBS987 and 0.511963 for the Rennes standard (Chauvel and Blichert-Toft, 2001), corresponding to a La Jolla value of 0.511858. Rb and Sr concentrations have been measured by X-ray fluorescence. The error on the Rb/Sr ratio is evaluated to be 4%. Sm and Nd concentrations were measured by ICP-MS. The Rb-Sr and Sm-Nd ages have been calculated following Ludwig (2001). Decay constants used (Steiger and Jäger, 1977) are $1.42 \times 10^{-11}\,a^{-1}$ (^{87}Rb) and $6.54\ 10^{-12}\,a^{-1}$ (^{147}Sm).

4. Field relationships and petrography

The Bessefjellet intrusion ($\approx 25\,km^2$) is a medium-grained ($\approx 2\,mm$) pink granite, grossly circular in shape and intrusive into the supracrustal formations (metabasalts, metasandstones and metarhyolites) of the Telemark Province (Dons, 1960; Killeen and Heier, 1975) (Fig. 1). It is homogeneous and generally displays a porphyritic texture with centimetric phenocrysts of perthitic microcline dispersed in a matrix essentially made of plagioclase, smaller grains of perthitic microcline, rounded quartz as well as minor biotite, apatite and accessory zircon, titanite and fluorite. Leucogranitic facies are abundant and

Table 4
Selected electron microprobe analyses of biotites

	Rustfjellet	Svöfjell	Verhuskjerringi	Valle	Bessefjellet
	R7	SV6	S2	VA1	BE1
SiO_2	38.04	37.25	38.65	38.50	39.44
TiO_2	2.80	2.57	2.47	1.30	2.10
Al_2O_3	15.20	14.27	12.44	13.40	13.95
FeO	18.61	20.76	17.93	18.06	17.01
MnO	0.44	0.43	0.78	0.64	0.50
MgO	10.87	11.72	14.18	13.58	13.30
CaO	0.00	0.03	0.00	0.00	0.00
Na_2O	0.06	0.03	0.10	0.05	0.05
K_2O	10.29	9.67	10.11	10.35	10.40
Cr_2O_3	0.00	0.05	0.00	0.05	0.00
F	1.39	0.63	1.96	2.55	1.71
Cl	0.11	0.20	0.09	0.15	0.08
H_2O%	3.29	3.60	3.04	2.71	3.20
OH–(F + Cl)	0.61	0.31	0.85	1.11	0.74
Total	100.49	100.90	100.90	100.23	101.00
Si	5.735	5.649	5.810	5.831	5.868
Ti	0.317	0.293	0.279	0.148	0.235
Al	2.702	2.551	2.205	2.393	2.447
Fe	2.346	2.633	2.254	2.288	2.117
Mn	0.056	0.055	0.099	0.082	0.063
Mg	2.442	2.649	3.177	3.065	2.949
Ca	0.000	0.005	0.000	0.000	0.000
Na	0.018	0.009	0.029	0.015	0.014
K	1.979	1.871	1.939	2.000	1.974
Cr	0.000	0.006	0.000	0.006	0.000
F	0.663	0.302	0.932	1.222	0.805
Cl	0.028	0.051	0.023	0.039	0.020
H_2O	3.309	3.646	3.045	2.740	3.175
Mg/(Mg + Fe)	0.510	0.502	0.585	0.573	0.582

contain secondary muscovite associated with fluorite. Locally, it is totally devoid of biotite. Aplitic and pegmatitic dykes crosscut the intrusion. It has been dated at 923 ± 16 Ma (Rb-Sr isochron) by Killeen and Heier (1975).

The Verhuskjerringi massif (≈50 km^2) is also almost circular and intrusive into the Telemark supracrustals (Fig. 1). The most common facies is a coarse-grained heterogranular (1 mm to 1 cm) granite containing perthitic microcline, plagioclase, quartz, biotite and locally amphibole as major phases. Zircon, apatite, titanite and opaques are accessory and titanite usually surrounds the opaques. The mafics (biotite, amphibole, opaque, apatite, zircon and titanite) commonly form aggregates of millimetric size. Some mesocratic and leucocratic facies are also present. The former is richer in biotite and amphibole containing relic cores of clinopyroxene, whereas secondary muscovite associated with fluorite have been observed in the latter. Aplitic dykes crosscut the intrusion.

The Rustfjellet pluton (≈15 km^2) straddles the MUL and is intrusive into the supracrustal formations of Telemark (metasandstones of the Bandak group) along its eastern margin and in the banded and granitic gneisses of the Rogaland-Vest Agder sector along its western margin. It is mainly leucogranitic but granitic facies also occur. Its texture is essentially equigranular with a variable grain size ranging from 1 to 5 mm. The major phases are plagioclase, quartz and perthitic microcline (containing inclusions of plagioclase and quartz) associated with minor biotite and secondary muscovite. Accessory phases are zircon,

Table 5
Selected electron microprobe analyses of clinopyroxenes

	Svöfjell			
	SV90-13	SV90-13	SV90-13	SV90-13
SiO_2	52.83	52.46	52.70	51.45
TiO_2	0.08	0.10	0.09	0.26
Al_2O_3	1.00	0.97	0.81	2.17
FeO	10.348	10.149	9.902	9.868
Fe_2O_3	1.842	2.481	1.933	3.744
MnO	0.92	0.93	0.93	0.82
MgO	11.51	11.13	11.33	11.31
CaO	22.79	23.16	23.46	20.97
Na_2O	0.45	0.48	0.43	0.61
K_2O	0.05	0.00	0.00	0.22
Total	101.82	101.86	101.58	101.47
Si	1.967	1.958	1.968	1.924
Al	0.044	0.043	0.036	0.096
Fe^{3+}	0.052	0.070	0.054	0.105
Fe^{2+}	0.322	0.317	0.309	0.309
Mg	0.639	0.620	0.631	0.630
Ca	0.910	0.926	0.939	0.840
Na	0.032	0.035	0.031	0.044
K	0.002	0.000	0.000	0.010
Ti	0.002	0.003	0.002	0.007
Mn	0.029	0.029	0.029	0.026
En	34.16	33.26	33.57	35.43
Fs	17.23	17.01	16.46	17.35
Wo	48.61	49.73	49.97	47.23

Fe^{3+} has been calculated using the method of Droop (1987).

apatite, opaque and fluorite. The latter mineral is usually interstitial and associated with muscovite. In some samples, the texture clearly suggests that muscovite was formed at the expense of biotite. Large enclaves of banded gneisses have been observed as well as some aplitic and pegmatitic dykes.

The Svöfjell massif is much larger than the other intrusions and covers around 350 km^2 (Fig. 1). It intrudes the various gneisses (banded, granitic and augen) of the Rogaland-Vest Agder sector. It has a coarse-grained equigranular to heterogranular texture with a grain size ranging from 1 to 10 mm. The composition is granodioritic to granitic and contains angular enclaves of the surrounding gneisses as well as scarce lobate microgranular mafic enclaves. The major phases are plagioclase, K-feldspar (perthitic microcline or orthoclase), quartz, brown to brown-green biotite and bluish green amphibole. Accessory phases are apatite, zircon and opaques commonly surrounded by titanite. The latter are usually present in aggregates together with biotite and amphibole. The Svöfjell massif is crosscut by aplitic and pegmatitic dykes. At several places, the granite is intrusive into migmatitic gneisses which locally display agmatitic textures. In these agmatites, slightly tilted blocks (m to dm) of gneisses are embedded in a leucocratic matrix. This leucocratic matrix (samples 84-59, 84-48, 84-50, SV90-6, SV90-8—called Svöfjell dykes hereafter) is very poor in mafics (biotite, orthopyroxene in samples 84-48, 84-59, SV90-6; apatite, zircon and opaques with locally a small amount of amphibole in samples 84-59, SV90-8). Some of these samples (84-48, 84-50, SV90-8) contain mesoperthites locally associated with plagioclase (84-50, SV90-8); the other ones contain antiperthitic plagioclase and perthitic K-feldspar (SV90-6, 84-59). Quartz is always abundant (>20%). The presence of orthopyroxene and mesoperthite in this leucocratic material suggests that it belongs to the charnockitic suite and is distinct from the main body of Svöfjell. Samples 84-52

Table 6
Major (wt.%: XRF data) and trace elements (ppm) compositions of a selection of samples

	Valle		Verhuskjerringi		Bessefjellet				Svöfjell					
	VA1	VA2	S1	S2	BE3	BE5	BE6	BE4	84-43	84-47	84-48	84-52	84-53	84-64
SiO_2	64.9	68.8	67.28	55.14	73.93	76.23	75.75	76.58	62.45	74.56	74.78	72.02	71.05	72.8
TiO_2	1.31	1.15	0.95	2.5	0.01	0.01	0.01	0.05	1.03	0.16	0.15	0.33	0.39	0.28
Al_2O_3	13.86	14.28	13.36	9.88	13.78	13.2	14.14	13.45	15.25	13.26	13.44	14.11	14.27	13.79
Fe_2O_3	3.75	2.69	3.64	–	0.54	0.43	0.37	0.74	3.76	1.33	0.73	1.48	1.81	1.55
FeO	2.23	1.06	1.78	15.14	0.26	0.39	0.32	0.24	2.64	0.57	0.72	1.18	1.21	1.22
MnO	0.11	0.19	0.12	0.33	0.07	0.11	0.07	0.04	0.1	0	0.04	0.06	0.01	0.03
MgO	1.32	0.2	0.84	2.63	0.22	0.14	0.15	0.06	1.6	0.38	0.51	0.82	0.83	0.54
CaO	3.35	2.17	3.44	5.02	1.15	0.32	0.09	0.19	4.56	0.46	0.75	0.88	1.04	0.74
Na_2O	3.75	4.08	3.18	1.5	3.18	3.49	3.93	4	3.19	2.31	3.54	3.2	3.43	2.99
K_2O	4.83	5.41	4.48	4.06	6.81	4.95	4.25	5.01	3.84	6.34	5.14	5.24	4.98	5.5
P_2O_5	0.39	0.01	0.32	1.69	0.01	0.01	0.01	0.01	0.53	0	0.03	0.07	0.11	0.05
Total	99.80	100.04	99.39	97.89	99.96	99.28	99.09	100.37	98.95	99.37	99.83	99.39	99.13	99.49
Agpaitic index	0.82	0.88	0.75	0.69	0.91	0.84	0.78	0.89	0.62	0.80	0.85	0.77	0.77	0.79
FeOt/MgO + FeOt	0.81	0.95	0.86	0.85	0.77	0.85	0.81	0.94	0.79	0.82	0.73	0.75	0.77	0.83
A/CNK	0.79	0.86	0.82	0.62	0.94	1.13	1.26	1.09	0.86	1.15	1.05	1.13	1.10	1.13
F	3119	1368	2009	–	6532	5665	4845	5111	–	–	–	–	–	–
U	2.6	2.9	4.6	6.4	9.8	4.3	6.7	16.3	2.7	5.7	11.7	7.6	3.5	5.5
Th	13.8	14.1	16.5	23.4	9.9	18.9	14.0	48.4	8.3	62.4	45.0	55.6	36.1	94.9
Zr	644	442	516	918	72	58	30	134	603	266	210	365	383	391
Hf	17.7	11.6	15.6	45.8	6.0	4.3	3.3	5.4	16.2	11.8	6.2	11.3	9.8	9.2
Ta	1.8	1.4	2.2	4.1	0.8	4.0	5.8	2.7	–	2.1	0.4	1.2	0.8	3.7
Nb	22	18	26	59	7	46	48	43	26	23	14	15	13	22
Zr/Hf	36	38	33	20	12	13	9	25	37	23	34	32	39	43
Th/U	5	5	4	4	1	4	2	3	3	11	4	7	10	17
Nb/Ta	12	13	12	14	9	11	8	16	–	11	33	13	16	6
Rb	141	244	188	201	527	714	843	746	125	282	337	288	279	323
Cs	0.86	0.68	3.49	5.16	3.88	3.43	4.56	4.57	2.68	1.65	0.98	0.84	0.91	1.77
Sr	814	397	471	283	95	34	28	38	670	226	106	257	264	271

Ba	2598	1394	1203	1123	128	104	44	103	1666	677	461	877	1053	784
Rb/Sr	0.2	0.6	0.4	0.7	5.5	21.0	30.1	19.6	0.2	1.2	3.2	1.1	1.1	1.2
Ga	28	25	25	26	25	24	40	30	29	22	23	24	24	42
Sc	11.6	4.1	10.8	31.6	2.4	10.8	13.4	11.8	–	–	–	–	–	–
V	65	29	37	–	–	–	–	–	56	12	12	32	40	25
Cr	21	–	19.5	22	–	3.1	4.4	9	–	–	–	–	–	–
Co	9.2	3.6	6.6	23.1	0.6	0.2		0.4	–	–	–	–	–	–
Ni	3.0	2.0	2.1	2.4	–	–	–	–	–	–	–	–	–	–
Zn	139	80	131	–	–	35	46	91	178	63	68	81	86	98
Pb	37	42	29	22	77	41	39	39	27	42	49	32	30	43
La	190	220	97	218	15	31	19	76	82	50	58	110	92	152
Ce	382	395	207	468	28	57	40	136	203	135	130	224	207	395
Pr	53.7	49.7	25.9	61.0	2.6	6.0	4.2	12.8	24.1	11.7	14.8	26.2	24.1	37.5
Nd	199	160	100	246	8	17	13	35	98	43	52	91	83	126
Sm	33.1	24.1	17.8	46.3	1.2	3.7	3.4	5.6	18.4	9.6	10.5	16.5	14.0	22.0
Eu	6.1	3.3	4.0	6.2	0.5	0.2	0.2	0.4	4.5	1.0	0.6	1.4	1.2	1.4
Gd	19.3	11.8	15.2	37.0	1.1	2.8	3.3	4.1	16.6	9.6	10.4	11.8	10.0	17.3
Tb	2.45	1.53	2.30	5	–	0.59	–	0.74	2.60	1.90	1.69	1.60	1.48	2.90
Dy	13.91	8.11	12.38	30.3	1.00	3.77	3.70	4.58	14.80	11.00	10.50	8.02	7.69	17.32
Ho	2.91	1.54	2.76	6.30	–	0.88	1.00	1.04	3.11	2.71	2.52	1.61	1.62	3.82
Er	6.70	3.63	7.16	15.8	0.70	2.60	2.90	3.20	7.54	6.76	6.86	3.33	3.54	9.94
Tm	1.02	0.54	1.07	2.3	0.14	0.59	0.60	0.66	1.09	1.10	1.24	0.48	0.47	1.67
Yb	5.72	2.79	7.24	14.8	1.1	5.05	5.2	5.05	7.25	7.26	7.38	2.83	2.70	9.40
Lu	0.82	0.38	1.03	2.3	0.20	0.89	1.20	0.86	1.07	0.96	1.16	0.39	0.41	1.22
Y	63	35	68	171	11	29	27	36	75	72	80	42	38	97
Y/Ho	22	23	25	27	–	33	27	34	24	27	32	26	23	25
$[La/Yb]_N$	23.8	56.6	9.6	10.6	9.8	4.3	2.6	10.8	8.1	4.9	5.6	27.9	24.4	11.6
[Eu/Eu*]	0.63	0.48	0.71	0.46	1.33	0.23	0.18	0.25	0.79	0.33	0.19	0.31	0.30	0.23

Table 6 (*Continued*)

	Svöfjell													
	SV1	SV2	SV3	SV4	SV5	SV6	SV7	SV8	SV9	SV10	SV11	SV12	SV13	SV90-13
SiO_2	61.98	61.44	62.36	61.4	64.4	65.31	62.25	63.1	65.23	61.23	62.82	62.06	64.31	59.13
TiO_2	1.46	1.34	1.47	1.29	0.79	1.27	1.56	1.21	1.48	2.05	1.72	1.7	1.12	1.36
Al_2O_3	15.06	15.4	14.77	15.42	16.48	14.77	14.67	15.55	14.78	14.13	14.61	15.52	16.3	15.8
Fe_2O_3	3.93	4.37	4.23	4.16	2.66	3.1	4.31	3.55	3.27	4.62	4.05	3.75	2.68	–
FeO	2.3	3.29	2.62	3.19	2.18	2.37	3.09	2.47	2.33	3.62	2.96	3.13	2.37	8.1
MnO	0.24	0.22	0.22	0.21	0.05	0.13	0.22	0.06	0.16	0.17	0.18	0.19	0.07	0.17
MgO	1.36	1.5	1.29	1.54	1.11	1.04	1.33	1.08	0.99	1.66	1.17	1.35	1.13	1.52
CaO	5.34	4.95	4.98	4.72	3.57	4.08	4.89	4.23	4.34	5.01	5.02	5.02	4.07	5.86
Na_2O	3.15	2.43	3.12	2.8	3.45	3.4	3.94	3.68	3.32	2.85	3.37	3.44	3.27	3.1
K_2O	3.38	3.62	3.57	3.72	3.8	4.18	3.9	3.58	3.89	3.79	3.67	3.63	3.7	2.78
P_2O_5	0.94	0.76	0.74	0.72	0.52	0.54	0.78	0.55	0.54	0.92	0.55	0.5	0.41	0.86
Total	99.14	99.32	99.37	99.17	99.01	100.19	100.94	99.06	100.33	100.05	100.12	100.29	99.43	99.94
Agpaitic index	0.59	0.51	0.61	0.56	0.59	0.68	0.73	0.64	0.65	0.62	0.65	0.62	0.58	0.51
FeOt/MgO + FeOt	0.81	0.83	0.83	0.82	0.80	0.83	0.84	0.84	0.84	0.82	0.85	0.83	0.81	0.80
A/CNK	0.81	0.91	0.82	0.90	1.01	0.84	0.75	0.88	0.84	0.79	0.78	0.83	0.97	0.84
F	1342	1751	1676	1752	1337	1429	2011	1947	1716	2143	1567	1669	1126	–
U	3.0	3.4	2.7	2.2	1.9	1.6	2.2	1.8	2.2	2.2	1.7	0.9	1.6	–
Th	8.9	10.0	8.0	6.4	5.7	4.6	6.8	5.2	5.9	6.4	5.7	2.8	5.0	–
Zr	535	720	674	734	605	655	851	722	654	712	757	707	528	713
Hf	14.6	21.3	17.3	22.1	16.2	17.0	18.8	18.6	16.5	22.9	17.9	17.9	16.7	–
Ta	1.5	2.2	1.8	1.6	1.2	1.3	1.6	1.8	1.5	1.9	1.7	1.5	1.3	–
Nb	24	29	27	29	22	20	30	31	23	28	29	26	21	27
Zr/Hf	37	34	39	33	37	39	45	39	40	31	42	39	32	–
Th/U	3	3	3	3	3	3	3	3	3	3	3	3	3	–
Nb/Ta	16	13	15	18	19	15	19	18	16	15	17	17	17	–
Rb	104	117	107	107	100	90	109	91	118	110	98	81	91	74
Cs	1.86	2.08	1.93	1.83	1.3	1.01	1.7	1.27	1.73	1.55	1.42	0.7	1.5	–
Sr	719	620	591	641	615	585	596	567	534	604	627	624	639	656
Ba	1384	1516	1495	1675	1946	1470	1555	1549	1483	1588	1673	1615	1667	1311

Rb/Sr	0.1	0.2	0.2	0.2	0.2	0.2	0.2	0.2	0.2	0.2	0.2	0.1	0.1	0.1
Ga	31	28	29	29	28	26	24	25	24	28	27	29	30	35
Sc	15.1	18.5	16.4	17	12.8	13.7	17.9	15.2	13.2	20	17.1	16.4	12.2	–
V	40	48	41	36	33	33	38	35	35	51	39	33	32	–
Cr	4.5	–	5.9	25.8	–	6	7.5	–	5	–	–	2.9	7.1	–
Co	7.3	10.2	8.4	9.2	6.1	6.4	8.5	6.5	6.2	9.4	8.2	8.4	6.0	–
Ni	–	1.6	–	1.0	–	–	–	–	–	–	–	2.0	1.0	–
Zn	158	187	173	178	134	148	199	163	153	225	181	179	137	–
Pb	23	24	23	34	21	25	25	27	20	25	19	20	24	–
La	82	97	88	87	75	81	92	84	66	122	83	82	65	–
Ce	178	214	200	192	164	168	209	191	167	255	184	188	144	–
Pr	–	29.0	–	–	–	23.7	–	–	–	39.0	–	–	18.0	–
Nd	–	123	–	–	–	99	–	–	–	163	–	–	82	–
Sm	17.4	25.1	19.8	20.6	15.1	20.0	21.3	19.8	18.4	32.0	19.2	18.7	15.6	–
Eu	5.6	5.7	5.2	5.3	5.3	5.9	5.2	5.1	4.7	7.5	5.3	5.1	4.5	–
Gd	–	21.0	–	–	–	17.2	–	–	–	28.6	–	–	13.0	–
Tb	2.22	2.5	2.54	2.7	1.94	2.56	2.73	2.65	2.45	4.07	2.52	2.42	1.91	–
Dy	–	17.90	–	–	–	13.03	–	–	–	22.47	–	–	11.20	–
Ho	–	3.70	–	–	–	3.02	–	–	–	4.62	–	–	2.60	–
Er	–	9.30	–	–	–	7.25	–	–	–	11.66	–	–	5.80	–
Tm	–	1.30	–	–	–	0.99	–	–	–	1.58	–	–	0.86	–
Yb	8	8.6	9.3	7.1	7.1	5.90	9.6	9.3	9.1	9.88	8.4	8.4	5.2	–
Lu	–	1.20	–	–	–	0.78	–	–	–	1.24	–	–	0.75	–
Y	–	101	–	–	–	70	–	–	–	108	–	–	67	–
Y/Ho	–	27	–	–	–	23	–	–	–	23	–	–	26	–
$[La/Yb]_N$	7.3	8.1	6.7	8.8	7.6	9.8	6.9	6.5	5.2	8.9	7.1	7.0	9.0	–
[Eu/Eu*]	1.18	0.94	0.96	0.93	1.28	1.08	0.88	0.92	0.91	0.86	0.99	0.99	0.97	–

Table 6 (*Continued*)

	Rustfjellet					Handeland						Aseral		
	R2	R3	R5	R6	R7	HA1	H7	H12	H14	H18	H22	A1	A5	A10
SiO_2	73.94	74.18	70.87	74.04	72.96	54.36	53.12	55.1	52.76	55.5	50.07	60.77	53.25	50.89
TiO_2	0.63	0.57	0.83	0.62	0.58	2.82	3.08	3.01	2.62	2.74	3.24	1.57	2.45	2.5
Al_2O_3	11.99	13.8	13.95	13.34	13.34	14.71	14.21	14.37	12.86	15.17	16.94	14.5	15.82	15.09
Fe_2O_3	1.3	0.93	2.02	1.49	1.74	4.8	5.81	5.4	7.39	4.45	5.46	5.15	6.57	6.55
FeO	0.65	0.34	0.75	0.54	0.6	6.65	6.14	6.3	7.13	6.45	6.52	2.69	4.19	5.44
MnO	0.06	0.09	0.15	0.21	0.07	0.15	0.15	0.15	0.19	0.14	0.15	0.1	0.13	0.16
MgO	0.23	0.35	0.46	0.15	0.35	4.8	3.23	3.82	3.31	3.32	4	2.03	3.77	5.24
CaO	1.06	0.95	1.56	1.32	1.15	5.75	8.03	6.58	7.33	6.87	7.76	4.27	6.66	7.33
Na_2O	3.53	3.64	3.85	3.46	3.41	2.86	2.33	2.61	2.32	2.67	2.97	2.86	2.28	2.78
K_2O	5.66	5.88	5.81	5.57	5.43	1.77	2.01	2.09	2.36	1.88	1.89	4.73	3.57	2.28
P_2O_5	0.15	0.08	0.14	0.22	0.12	1.12	1.75	1.15	1.53	1.09	1.02	0.7	1.42	1.39
Total	99.20	100.81	100.39	100.96	99.75	99.79	99.86	100.58	99.80	100.28	100.02	99.37	100.11	99.65
Agpaitic index	1.00	0.90	0.90	0.88	0.86	0.45	0.42	0.46	0.50	0.42	0.41	0.68	0.48	0.47
FeOt/MgO + FeOt	0.89	0.77	0.85	0.93	0.86	0.70	0.78	0.75	0.81	0.76	0.74	0.78	0.73	0.68
A/CNK	0.87	0.98	0.90	0.94	0.98	0.86	0.69	0.78	0.65	0.80	0.81	0.82	0.80	0.74
F	–	2377	4759	4237	2495	–	–	–	–	–	–	–	–	–
U	4.0	5.3	9.0	7.3	3.6	1.8	1.0	1.3	1.2	2.6	0.9	3.2	1.7	1.0
TH	39.3	53.3	41.2	89.4	39.2	2.8	3.1	3.4	3.8	5.7	2.6	13.3	5.2	5.3
Zr	258	158	373	266	328	306	320	300	354	325	251	548	283	241
Hf	7.9	6.2	11.5	9.5	10.9	6.9	7.0	6.8	7.9	7.7	5.9	13.4	6.8	6.1
Ta	0.2	0.7	1.2	0.7	1.0	0.86	0.97	0.81	1.10	1.08	0.86	2.07	0.73	0.64
Nb	9	8	34	9	13	18	18	14	22	19	17	32	13	11
Zr/Hf	33	25	32	28	30	45	45	44	45	42	43	41	42	39
Th/U	10	10	5	12	11	1.6	3.2	2.5	3.1	2.2	2.8	4.2	3.1	5.5
Nb/Ta	39	12	29	13	13	21	18	18	20	18	20	16	18	17
Rb	272	295	353	270	261	66	47	68	62	63	63	168	124	56
Cs	1.42	1.26	2.04	1.3	1.36	1.76	0.42	0.89	0.53	1.14	1.03	0.86	0.81	0.46
Sr	254	197	281	239	281	615	753	661	699	668	765	796	1405	1392

Ba	712	460	1016	641	812	891	1014	934	1193	651	724	2233	2001	1652
Rb/Sr	1.1	1.5	1.3	1.1	0.9	0.11	0.06	0.10	0.09	0.09	0.08	0.21	0.09	0.04
Ga	23	24	25	23	28	24	24	23	29	23	25	26	25	22
Sc	4	2.3	7.5	3.2	3.6	–	–	–	–	–	–	–	–	–
V	12	12	12	12	25	220	196	211	183	205	233	100	197	244
Cr	–	–	–	4.7	–	47	35	28	2.7	39	17	28	36	64
Co	1.7	0.6	2.6	1.5	2.3	36	29	34	41	28	28	12	25	32
Ni	0.3	–	0.6	–	–	46	10	31	6	33	33	12	12	32
Zn	48	42	78	55	56	153	167	189	230	158	180	141	164	181
Pb	80	81	79	77	69	13.4	13.9	19.8	25.8	19.2	13.6	35.8	35.7	35.5
La	126	51	154	124	176	59	69	61	84	69	62	151	110	126
Ce	214	100	282	222	279	141	162	138	196	155	138	358	227	261
Pr	18.0	9.6	26.9	20.0	23.9	18	21	18	26	20	18	43	26	31
Nd	55	29	83	60	67	77	91	73	111	83	76	155	106	122
Sm	6.4	3.6	12.7	6.9	7.8	14.9	17.9	14.4	21.8	15.8	15.4	25.5	17.0	18.5
Eu	1.0	0.7	1.6	1.1	1.1	3.5	4.3	3.5	4.9	3.7	3.5	4.6	4.2	4.2
Gd	3.2	2.4	9.7	4.4	4.9	11.5	14.4	11.3	17.1	12.6	12.1	17.9	12.2	12.3
Tb	–	0.29	1.36	0.55	0.73	1.7	2.0	1.7	2.5	1.9	1.8	2.5	1.6	1.6
Dy	2.00	1.98	7.54	3.10	3.22	8.8	10.3	8.4	12.9	9.6	9.3	13.0	7.3	7.2
Ho	0.40	0.52	1.79	0.80	0.71	1.7	2.0	1.7	2.5	1.9	1.8	2.6	1.3	1.3
Er	1.20	1.53	4.88	2.00	1.87	4.5	5.1	4.3	6.5	4.9	4.7	6.6	3.2	3.1
Tm	0.19	0.29	0.72	0.31	0.31	0.57	0.68	0.55	0.82	0.67	0.63	0.94	0.39	0.40
Yb	1.2	2.12	4.75	2	2.06	3.91	4.39	3.49	5.30	4.41	4.02	5.97	2.24	2.51
Lu	0.20	0.36	0.60	0.33	0.31	0.56	0.62	0.49	0.67	0.64	0.56	0.79	0.30	0.33
Y	12	15	50	24	18	49	57	44	70	50	50	70	36	33
Y/Ho	30	30	28	30	26	29	28	26	28	27	27	27	27	26
$[La/Yb]_N$	75.3	17.1	23.2	44.5	61.4	10.9	11.3	12.5	11.4	11.2	11.0	18.1	35.2	35.9
[Eu/Eu*]	0.68	0.71	0.45	0.61	0.56	0.83	0.81	0.83	0.78	0.81	0.78	0.66	0.88	0.85

Table 6 (*Continued*)

	Holum													
	9B	2A	41C	25C	93C	39B	46C	58C	99D	33C	81C	100C	72D	6
SiO_2	68.22	64.13	63.38	63.95	64.53	64.85	65.49	65.50	65.72	65.86	66.36	66.64	66.98	66.83
TiO_2	0.73	1.06	1.11	1.03	0.97	0.96	0.94	0.97	0.68	0.85	0.83	0.81	0.83	0.75
Al_2O_3	14.71	14.31	14.14	14.18	14.42	14.14	13.83	13.89	15.38	14.00	14.45	14.10	14.35	14.32
Fe_2O_3	–	–	–	–	–	–	–	–	–	–	–	–	–	–
FeO	4.06	5.62	6.06	5.47	5.72	5.55	5.45	5.65	3.90	4.67	5.08	4.91	4.54	5.04
MnO	0.10	0.12	0.12	0.11	0.10	0.13	0.12	0.13	0.08	0.09	0.10	0.09	0.07	0.11
MgO	0.72	1.25	0.98	0.98	0.92	0.91	0.99	1.08	0.82	0.77	0.80	0.97	0.98	0.86
CaO	3.23	3.50	3.91	3.80	3.49	3.72	3.39	3.27	3.17	3.32	3.14	2.72	2.88	3.00
Na_2O	3.08	3.36	3.92	3.54	3.77	3.55	2.91	3.34	4.47	3.56	3.65	3.28	3.55	3.43
K_2O	4.18	4.43	4.20	4.34	4.36	3.97	4.58	4.24	4.61	4.54	4.42	4.48	4.24	3.97
P_2O_5	0.47	0.59	0.77	0.59	0.49	0.53	0.54	0.61	0.38	0.47	0.35	0.45	0.31	0.59
Total	99.50	98.37	98.59	97.99	98.77	98.31	98.22	98.68	99.21	98.13	99.18	98.45	98.73	98.90
Agpaitic index	0.65	0.72	0.78	0.74	0.76	0.72	0.70	0.73	0.80	0.77	0.75	0.73	0.73	0.69
FeOt/MgO + FeOt	0.85	0.82	0.86	0.85	0.86	0.86	0.85	0.84	0.83	0.86	0.86	0.84	0.82	0.85
A/CNK	0.95	0.86	0.78	0.81	0.84	0.84	0.87	0.87	0.85	0.83	0.88	0.93	0.92	0.93
F	–	–	–	–	–	–	–	–	–	–	–	–	–	–
U	0.7	1.9	0.9	1.4	1.4	1.1	1.6	1.4	1.6	1.7	1.4	1.9	2.1	1.1
TH	6.2	13	6.7	12	9.5	8.1	12	11	12	11	11	14	19	7.0
Zr	–	–	–	–	–	–	–	–	470	699	580	632	653	914
Hf	16	16	19	17	14	20	24	23	19	15	17	16	19	16
Ta	1.5	2.0	1.6	1.9	1.4	1.5	2.7	2.2	1.6	1.5	1.5	1.7	1.6	1.5
Nb	35	39	31	31	19	37	39	35	16	25	19	21	19	30
Zr/Hf	58	58	52	48	37	53	45	42	25	47	33	38	35	57
Th/U	9.1	6.8	7.4	8.2	6.7	7.3	7.6	7.9	7.7	6.4	7.9	7.4	9.1	6.6
Nb/Ta	23	19	20	16	14	24	14	16	10	16	13	12	12	20
Rb	112	134	97	108	109	110	153	122	115	118	106	119	128	141
Cs	0.26	0.32	0.41	0.26	0.48	0.31	0.67	0.31	1.4	0.56	0.36	1.4	0.88	0.47

Sr	575	640	730	725	518	566	447	485	784	675	501	532	456	476
Ba	2375	2133	2561	2544	2544	2099	2176	2209	1758	2453	1940	2081	1753	1851
Rb/Sr	0.19	0.21	0.13	0.15	0.21	0.19	0.34	0.25	0.26	0.18	0.21	0.24	0.28	0.30
Ga	29	30	28	26	24	30	30	26	23	26	24	23	22	29
Sc	–	–	–	–	–	–	–	–	–	–	–	–	–	–
V	19	48	40	35	17	26	25	19	11	28	17	16	23	31
Cr	–	–	–	–	–	–	–	–	–	–	–	–	–	–
Co	5.2	8.9	7.9	6.1	3.9	7.1	5.8	4.9	5.3	5.7	4.6	4.2	4.3	6.4
Ni	–	–	–	–	–	–	–	–	–	–	–	–	–	–
Zn	187	190	140	135	95	192	192	165	82	129	122	117	101	173
Pb	30	27	24	28	33	27	30	32	93	27	30	100	27	25
La	158	161	148	167	96	157	146	143	147	136	114	151	141	143
Ce	319	351	323	352	211	345	362	331	298	292	250	305	292	265
Pr	43.4	46.7	43.6	46.5	28.1	47.6	53.2	46.6	38.6	39.3	33.6	46.2	37.5	43.3
Nd	163	175	167	173	109	189	215	184	180	146	132	183	137	164
Sm	29.2	30.1	30.0	30.1	19.1	34.4	42.5	35.6	27.2	25.1	23.9	34.0	23.0	30.5
Eu	6.5	5.4	6.4	5.9	4.2	7.4	7.3	7.0	5.6	5.2	5.2	5.9	4.1	5.4
Gd	23.3	22.0	22.7	22.5	15.3	27.8	34.7	29.9	27.8	19.7	19.5	29.4	16.6	24.1
Tb	3.7	3.6	3.3	3.7	2.8	4.0	5.2	4.3	4.1	2.7	2.8	5.0	2.4	396.0
Dy	19.5	18.0	17.7	17.7	11.6	22.8	30.4	25.0	24.1	15.3	16.7	24.4	12.8	20.9
Ho	3.8	3.6	3.6	3.4	2.3	4.5	6.0	5.0	4.9	2.9	3.2	4.6	2.4	391.0
Er	10.4	9.3	9.1	9.1	6.1	11.9	16.6	13.6	13.5	7.9	9.0	12.3	6.6	11.1
Tm	1.5	1.3	1.3	1.3	0.8	1.6	2.3	1.9	2.4	1.1	1.2	1.6	1.0	1.5
Yb	9.3	8.1	7.7	7.9	5.6	10.1	15.0	12.2	13.4	7.0	7.9	9.9	6.1	9.5
Lu	1.4	1.2	1.1	1.2	0.8	1.5	2.1	1.8	2.2	1.0	1.2	1.4	0.8	1.4
Y	117.2	105.7	94.7	87.7	51.1	121.8	152.4	116.3	80	75	67	102	51	125
Y/Ho	31	30	26	26	22	27	25	23	16	26	21	22	21	0
$[La/Yb]_N$	12	14	14	15	12	11	7.0	8.4	7.9	14	10	11	17	11
[Eu/Eu*]	0.76	0.65	0.75	0.69	0.75	0.73	0.58	0.66	0.62	0.71	0.73	0.57	0.64	0.60

Table 6 (*Continued*)

	Holum						Holum enclaves		
	65C	39A	44C	11	90C	50C	73C	31C	21E
SiO_2	68.47	70.37	69.38	69.88	70.12	71.08	72.48	72.86	71.61
TiO_2	0.71	0.36	0.61	0.29	0.43	0.45	0.46	0.41	0.17
Al_2O_3	13.64	15.09	13.52	14.77	13.45	13.28	13.57	13.51	14.57
Fe_2O_3	–	–	–	–	–	–	–	–	–
FeO	4.22	2.20	3.54	2.18	3.40	2.98	3.19	2.86	1.40
MnO	0.08	0.06	0.07	0.04	0.06	0.06	0.06	0.06	0.02
MgO	0.66	0.54	0.62	0.30	0.61	0.31	0.53	0.55	0.37
CaO	2.69	2.01	2.40	1.37	1.28	1.34	1.90	1.76	1.53
Na_2O	3.35	3.22	2.88	3.65	3.80	3.20	3.17	3.20	3.66
K_2O	4.32	5.41	4.77	5.68	5.23	5.66	4.03	4.26	5.57
P_2O_5	0.40	0.08	0.38	0.07	0.12	0.15	0.14	0.13	0.06
Total	98.54	99.36	98.19	98.23	98.50	98.51	99.52	99.60	98.96
Agpaitic index	0.75	0.74	0.73	0.82	0.89	0.86	0.71	0.73	0.83
FeOt/MgO + FeOt	0.86	0.80	0.85	0.88	0.85	0.91	0.86	0.84	0.79
A/CNK	0.90	1.02	0.95	1.01	0.94	0.96	1.04	1.03	0.98
F	–	–	–	–	–	–	–	–	–
U	1.3	0.34	1.1	0.4	2.6	0.8	2.5	1.6	0.6
Th	7.0	4.1	6.3	5.7	43	27	13	7.6	8.8
Zr	574	253	530	229	340	406	202	212	150
Hf	15	5	12	4.7	10	12	6.7	5.7	3.8
Ta	1.4	0.4	1.8	0.21	1.9	0.91	1.3	0.71	0.14
Nb	20	13	27	4.8	13	18	11	11	3.6
Zr/Hf	39	47	45	49	33	35	30	37	40
Th/U	5.4	12.2	5.8	15	17	33	5.1	4.7	14
Na/Ta	14	28	15	23	6.9	20	8.5	15	26
Rb	102	136	132	146	202	169	136	125	128
Cs	0.46	0.21	1.0	0.55	0.83	0.28	1.0	0.71	0.33
Sr	529	639	474	510	271	200	109	129	362
Ba	2064	2908	2415	1457	1176	964	564	669	818
Rb/Sr	0.19	0.21	0.28	0.29	0.75	0.86	1.3	1.0	0.34
Ga	23	25	25	22	22	23	19	20	21

Sc	–	–	–	–	–	–	–	–	–
V	14	8	16	25	14	7	17	21	13
Cr	–	–	–	–	–	–	–	–	–
Co	4.1	2.7	4.1	4.0	3.0	3.0	3.7	4.4	2.8
Ni	–	–	–	–	–	–	–	–	–
Zn	95	91	121	100	97	80	67	62	40
Pb	27	34	32	34	32	27	28	31	31
La	89	78	116	52	98	187	51	65	39
Ce	224	150	272	391	187	387	104	111	67
Pr	29.4	18.8	40	11	24	47	13	13	7
Nd	114	72	154	35	82	156	48	43	22
Sm	20.9	12.5	29.3	5.2	15.1	25.6	9.8	6.0	2.2
Eu	4.8	4.6	6.1	1.4	2.6	3.1	1.8	1.7	0.7
Gd	16.9	9.7	23.8	3.7	12.0	18.6	8.7	4.9	1.4
Tb	2.5	1.4	3.5	1.4	1.8	2.7	1.4	1.4	1.1
Dy	13.8	7.7	20.9	2.5	10.3	14.4	8.2	3.3	0.7
Ho	2.7	1.5	4.1	0.5	2.2	2.7	1.8	0.7	0.2
Er	7.4	3.9	11.3	1.2	5.9	7.0	5.0	1.9	0.3
Tm	1.0	0.6	1.5	0.2	0.9	1.0	0.8	0.3	0.1
Yb	6.7	3.4	9.9	1.0	6.2	5.7	5.1	2.1	0.5
Lu	1.0	0.5	1.4	0.1	0.9	0.8	0.8	0.4	0.1
Y	61	40	107	15	48	60	38	18	5
Y/Ho	23	27	26	31	22	22	22	27	31
$[La/Nb]_N$	10	17	8.4	37	11	23	7	22	57
[Eu/Eu*]	0.77	1.27	0.70	0.96	0.59	0.43	0.58	0.93	1.14

Table 6 (*Continued*)

	Gneisses							Gabbronorite
	VDA 9902	VDA 9903C	VDA 9903F	VDA 9904	VDA 9905	VDA 9906	VDA 9907	Sko2*
SiO_2	52.62	69.98	49.80	73.13	51.27	73.56	68.46	52.35
TiO_2	2.30	0.70	1.90	0.42	1.02	0.42	0.64	2.12
Al_2O_3	14.08	13.15	13.88	12.95	15.34	13.23	13.02	17.31
Fe_2O_3	13.97	5.13	15.22	2.90	11.52	3.23	6.57	3.41
FeO	–	–	–	–	–	–	–	6.25
MnO	0.20	0.07	0.25	0.04	0.18	0.04	0.11	0.15
MgO	3.88	0.62	5.90	0.30	6.44	1.02	2.07	6.2
CaO	7.07	2.46	8.54	1.46	9.02	2.70	4.31	7.34
Na_2O	3.85	2.86	3.15	2.76	3.57	4.26	3.28	3.49
K_2O	0.87	4.35	0.83	5.21	0.89	0.86	0.85	1.34
P_2O_5	0.52	0.16	0.20	0.07	0.24	0.09	0.10	0.5
Total	99.36	99.48	99.67	99.22	99.49	99.41	99.41	100.46
Agpaitic index	0.52	0.72	0.44	0.79	0.45	0.60	0.48	0.42
FeOt/MgO + FeOt	0.76	0.88	0.70	0.90	0.62	0.74	0.74	0.33
A/CNK	0.70	0.95	0.64	1.01	0.66	1.03	0.92	0.84
F	–	–	–	–	–	–	–	–
U	0.20	1.07	1.85	1.04	0.72	0.70	2.37	0.69
Th	0.30	2.27	2.75	10.5	1.56	4.87	5.34	2.5
Zr	170	562	111	327	93	286	187	204
Hf	5	16	3	9	3	7	5	4.23
Ta	0.71	0.53	0.73	0.67	0.31	0.33	0.90	0.77
Nb	11	13	7	12	5	6	10	7
Zr/Hf	34	36	33	35	36	40	37	48
Th/U	2	2	1	10	2	7	2	4
Na/Ta	16	24	9	17	16	20	11	9
Rb	11	124	17	151	13	13	41	30
Cs	0.05	0.08	0.07	0.15	0.23	0.14	1.65	–
Sr	228	120	120	82	104	105	119	508
Ba	290	793	98	878	291	374	254	365
Rb/Sr	0.05	1.04	0.14	1.83	0.12	0.12	0.34	0.06
Ga	22	19	23	19	21	14	17	–

Sc	–	–	–	–	–	–	–	16.7
V	–	–	–	–	–	–	–	–
Cr	–	–	–	–	–	–	–	133
Co	35	7	46	3	47	6	14	42.8
Ni	–	–	–	–	–	–	–	90.0
Zn	171	99	173	51	112	31	85	98
Pb	6	14	7	18	3	3	10	–
La	32	40	38	51	13	33	24	20
Ce	76	88	104	108	29	73	56	46
Pr	10	10	13	12	3.81	8.47	7.20	–
Nd	43	44	53	49	17	33	30	27
Sm	9.9	10	13	9.4	4.0	7.0	6.7	6.0
Eu	2.2	2.0	2.3	1.6	1.4	1.4	1.3	2.0
Gd	10	11	12	8.57	4.44	5.98	7.09	–
Tb	1.65	1.80	2.19	1.36	0.75	0.90	1.21	0.88
Dy	9.41	11	14	7.34	4.35	4.56	7.79	–
Ho	–	–	–	–	–	–	–	–
Er	5.16	5.78	8.08	3.82	2.61	2.40	4.99	–
Tm	0.78	0.85	1.26	0.54	0.41	0.37	0.79	-
Yb	5.06	5.62	8.44	3.38	2.60	2.47	5.39	2.36
Lu	0.71	0.82	1.23	0.46	0.38	0.37	0.78	0.34
Y	54	58	87	40	28	28	57	29
Y/Ho	–	–	–	–	–	–	–	–
$[La/Nb]_N$	5	5	3	11	4	10	3	5.99
[Eu/Eu*]	0.66	0.59	0.56	0.55	0.98	0.65	0.57	1.14

Rb, Sr, Ba, Zn by XRF; V, Sc, Cr, Co, Ni by INAA; U, Th, Hf, Ta, Cs: INAA except for 84-43,84-47,84-48,84-52,84-53,84-64; REE by ICP-MS except for SV1, SV3 to SV5, SV7 to SV9, SV11, SV12 (INAA); Y by ICP-MS; Zr by XRF except for BE5, BE4 (INAA); Ga by XRF except for BE3 to BE6, 84-64; Pb by ICP-MS except for BE5, SV1, SV3 to SV5, SV7 to SV9, SV11, SV12; Nb by XRF except for BE4, BE5, VA1, VA2, 84-43, 84-47, 84-48, 84-52, 84-53, 84-64, SV6, SV10, S1, R3, R5, R7. F determined by PIGE (Roelandts et al., 1987). For samples of Holum (sample number have a 98BN prefix): Rb, Sr average of XRF and ICP-MS values, other trace elements by ICP-MS.
* Demaiffe et al. (1990).

Table 7
Sr and Nd isotopic data for the HBG suite

Pluton	Sample	Rb (ppm)	Sr (ppm)	$^{87}Rb/^{86}Sr$	$^{87}Sr/^{86}Sr$	2σ	Sr^{i} (930 Ma)	Sm (ppm)	Nd (ppm)	$^{147}Sm/^{144}Nd$	$^{143}Sm/^{144}Nd$	2σ	Nd^{i} (930 Ma)	ε_{Nd} (930 Ma)	Model ages (Nelson and De Paolo, 1984)
Bessefjellet	BE4	746	38	61.7	1.576833	0.000040	0.756893	5.6	35	0.09675	0.511830	0.000028	0.511240	−3.88	1564
	BE5	714	34	66.2	1.612856	0.000050	0.732892	3.7	17	0.13162	0.511908	0.000007	0.511105	−6.51	2187
Valle	VA1	141	814	0.501	0.710835	0.000050	0.704169	33.1	199	0.10058	0.511852	0.000007	0.511238	−3.90	1581
	VA2	244	397	1.782	0.728681	0.000020	0.704989	24.1	160	0.09108	0.511743	0.000012	0.511187	−4.90	1595
Svöfjell	84-43	125	670	0.540	0.711840	0.000040	0.704660	18.4	98	0.09971					
	84-47	282	226	3.627	0.752138	0.000020	0.703927	9.6	43	0.11856					
	84-64	323	271	3.464	0.750723	0.000040	0.704678	22	126	0.09272					
	SV6	90	585	0.445	0.711511	0.000030	0.705590	20.0	99	0.12217	0.512121	0.000011	0.511376	−1.22	1509
	SV10	110	604	0.527	0.711925	0.000040	0.704916	32.0	163	0.11872	0.512117	0.000018	0.511393	−0.89	1458
Svöfjell/dykes	84-48	337	106	9.318	0.837726	0.000080	0.713855	10.5	52.0	0.12211	0.512119	0.000009	0.511374	−1.25	1511
	84-52	288	257	3.257	0.753079	0.000030	0.709777	16.5	91	0.09629					
	84-53	279	264	3.070	0.748356	0.000010	0.707538	14	83	0.10200	0.512017	0.000008	0.511395	−0.85	1394
Verhuskjerringi	S1	188	471	1.156	0.719226	0.000040	0.703854	17.8	100	0.10764	0.512060	0.000007	0.511403	−0.68	1387
Rustfjellet	R3	295	197	4.356	0.761137	0.000020	0.703228	3.6	29	0.07507	0.511743	0.000021	0.511285	−2.99	1426
	R5	353	281	3.651	0.751288	0.000040	0.702754	12.7	83	0.08126					
	R7	261	281	2.696	0.738589	0.000010	0.702740	7.8	67	0.07040	0.511672	0.000051	0.511243	−3.82	1420
Holum	98BN25C	108	725	0.431	0.710394	0.000011	0.704662	28	152	0.11140	0.511957	0.000008	0.511277	−3.14	1614
	98BN93C	109	518	0.609	0.712373	0.000010	0.704274	32.4	161	0.12170	0.512057	0.000009	0.511315	−2.41	1629
	98BN33C	118	675	0.506	0.711353	0.000010	0.704626	25.2	134	0.11373	0.511983	0.000007	0.511289	−2.91	1612
	98BN100C	119	532	0.648	0.713465	0.000008	0.704855	31.9	172	0.11216	0.512037	0.000010	0.511353	−1.67	1507
	98BN44C	131	474	0.800	0.715138	0.000010	0.704498	34.3	167	0.12421	0.512061	0.000007	0.511303	−2.63	1668
	98BN50C	169	200	2.452	0.737252	0.000009	0.704651	27	162	0.10079	0.511965	0.000009	0.511350	−1.72	1452
Holum/incl	98BN21E	115	339	0.983	0.719857	0.000010	0.706791	2.75	22.3	0.07457	0.511786	0.000009	0.511331	−2.09	1376
Gneisses	VDA 9902	11	228	0.142	0.710529	0.000027	0.708635	9.9	42.6	0.14113	0.512212	0.000008	0.511351	−1.70	1739
	VDA 9905	13	104	0.360	0.713619	0.000014	0.708837	4.0	17.0	0.14344	0.512321	0.000012	0.511446	0.16	1560
	VDA 9906	13	105	0.355	0.713082	0.000010	0.708359	7.0	33.3	0.12683	0.512053	0.000008	0.511279	−3.10	1732
	VDA 9907	41	119	0.991	0.721119	0.000010	0.707950	6.7	29.8	0.13522	0.512222	0.000012	0.511397	−0.80	1589
	VDA 9903C	124	120	3.020	0.773236	0.000023	0.733095	10.1	44.4	0.12108					
	VDA 9903F	17	120	0.403	0.723119	0.000010	0.717767	12.7	53.0	0.14445	0.512262	0.000029	0.511381	−1.12	1712
	VDA 9904	151	82	5.368	0.827010	0.000013	0.755645	9.4	48.9	0.11609	0.512059	0.000010	0.511351	−1.71	1533

and 84-53 have been sampled at the northern contact of the Svöfjell massif and according to the 1:250,000 geological map, could belong to a separate intrusion.

The granodioritic to granitic intrusion of Valle (≈150 km^2) displays a porphyritic texture with phenocrysts (several cm) of perthitic microcline embedded in a matrix of plagioclase, microcline, quartz, green biotite and bluish-green amphibole ranging in size from 0.25 to 2 mm. Biotite is much more abundant than amphibole. The microcline phenocrysts contain inclusions of quartz, biotite and plagioclase displaying an albitic rim at the contact with the K-feldspar. Titanite, zircon, apatite and opaques are accessory phases. This intrusion contains lobate mafic microgranular enclaves which together with the microcline phenocrysts are locally slightly oriented, probably due to magmatic flow.

The Holum granite outcrops close to the southernmost tip of the MUL (Fig. 1). It forms a north-south elongated pluton (≈83 km^2) intruded into banded, granitic and augen gneisses of the Rogaland-Vest Agder sector, metamorphosed under amphibolite-facies. As already noticed by Wilson et al. (1977), no metamorphic aureole can be detected around the granite. Xenoliths from the country rocks are found throughout the pluton, the most abundant being several centimeters to hundred of meters size enclaves of faintly-foliated biotite–granite, presumably coming from the granitic gneisses. Mafic microgranular enclaves have not been found. Pegmatite veins occur, especially along the margins of the pluton. The main rock-forming minerals are K-feldspar (usually microperthitic microcline), unzoned plagioclase, quartz, reddish-brown biotite, and green-brown hornblende. Opaque phases (magnetite, subordinate pyrite, and trace of hemo-ilmenite), notably abundant titanite often rimming magnetite, zoned zircon, apatite, and sporadic fluorite and allanite occur as accessory minerals. Biotite is usually more abundant than hornblende, and the mafic minerals constitute about 5–25% of the rock. Mineral modal proportions indicate almost exclusively monzogranitic compositions. The rock is usually coarse-grained (average grain size about 2–3 mm) and displays an heterogranular hypidiomorphic texture, with frequent K-feldspar and/or plagioclase phenocrysts up to 1.5–2 cm long. The mafic minerals tend to form more or less elongated aggregates, up to several millimetres long. The Holum granite is considered to be the oldest Sveconorwegian posttectonic granite of southernmost Norway and its emplacement age (980 Ma, based on a Rb-Sr whole-rock isochron: Wilson et al., 1977) is usually taken as a lower limit for the last Sveconorwegian regional folding phase in the area (Falkum, 1998). A recent structural study of the Holum granite, based on a survey of its anisotropy of low-field magnetic susceptibility, has shown, however, that this pluton is not posttectonic, but that it was emplaced in a tectonic strain field (Bolle et al., in press). A model of emplacement and deformation synchronous with the last Sveconorwegian regional folding phase evidenced in southernmost Norway, has been proposed (Bolle et al., in press).

The small intrusions of Handeland (≈2 km^2) and Åseral (≈5 km^2) were emplaced at a short distance south of Svöfjell (Fig. 1) and their mineralogy is similar to that of the main granites. The Handeland body is essentially quartz dioritic with biotite and hornblende as the main mafic phases as well as plagioclase and quartz. Relics of clinopyroxene partly reacted to hornblende are often present and can be abundant. Apatite, zircon and opaque(s), usually surrounded by titanite, are accessory phases. In the Åseral intrusion, composition ranges from quartz monzonite to granite. The major phases are plagioclase, K-feldspar (often microcline), quartz, biotite and hornblende. Accessory phases include opaque(s), usually surrounded by a rim of titanite, apatite, zircon and common fluorite.

The Lyngdal hyperites include the most mafic samples of the granitoid series and have been described by Demaiffe et al. (1990). Hyperite is an old swedish name for a rock composed of hypersthene, plagioclase and augite and its application has been restricted to Scandinavia (Demaiffe et al., 1990). In the rocks discussed here, pyroxenes (orthopyroxene, clinopyroxene) are the dominant mafic minerals associated with rare amphibole, biotite is a minor phase. Ilmenite, magnetite, apatite, K-feldspar, quartz and pyrite are accessory minerals (Demaiffe et al., 1990). Using the exact IUGS terminology (Streckeisen, 1976), these samples will be called gabbronorites. Similar rocks have been described in the Laramie Anorthosite Complex (Fuhrman et al., 1988; Kolker and Lindsley, 1989) and named biotite gabbros or high-Al gabbros (Mitchell et al., 1995). The belonging of these gabbronorites to the granitoid series is discussed in detail in Section 8.1.

5. Mineral chemistry

Plagioclase composition (Table 2) ranges from An_{15} (Bessefjellet) up to An_{31} (Svöfjell, Verhuskjerringi), An_{50} (Handeland: optical determination) and An_{58} (Lyngdal gabbronorites: Demaiffe et al., 1990). The amphibole (Table 3) present in Valle, Verhuskjerringi and Svöjell is an edenitic to magnesian hastingitic hornblende (Leake, 1978) with a fluorine content ranging from 0.50 wt.% (Svöfjell) up to 1.06 wt.% (Valle). In the Lyngdal gabbronorites, the secondary amphibole is a ferroan pargasitic hornblende (Demaiffe et al., 1990). Biotite is richer in fluorine than amphibole with contents ranging from 0.63 wt.% (Svöfjell) up to 2.55 wt.% (Valle) (Table 4). Its Fe# ranges from 0.4 up to 0.56 for an Al content of 2.2 up to 2.8 per formula unit. This biotite lies on the lower part of the X_{Fe} versus Al pfu trend of biotites from 1.4 Ga granites in the southwest USA (Anderson, 1987; Frost et al., 1999). Relic cores of clinopyroxene are salite with an average composition of $En_{34}Fs_{17}Wo_{49}$ (Table 5). In the Lyngdal gabbronorites, the pyroxenes have the following average compositions: $En_{39}Fs_{13}Wo_{48}$ (salite), $En_{58}Fs_{41}Wo_{1}$ (hypersthene) (Demaiffe et al., 1990).

6. Geochemistry

6.1. Nomenclature

In the cationic classification of Debon and Le Fort (1983) (Fig. 2A), samples define a whole series, intermediate between the CALK (calc-alkaline) and SALKD (dark subalkaline potassic) trends, and stretching from the gabbro to the granite fields. Samples of the dykes crosscutting the agmatites in the surrounding gneisses of Svöfjell fall in the granite (84-48, 84-50), adamellite (SV90-6, SV90-8) and tonalite (84-59) fields. Most samples are metaluminous (A/CNK $<$ 1: see Table 6) whereas a group of samples from Svöfjell, Verhuskjerringi (not shown in Table 6), Rustfjellet (not shown in Table 6) and Bessefjellet are slightly peraluminous.

The granitoids plot in the subalkaline field in a TAS ($Na_2O + K_2O$ versus SiO_2) diagram (not shown) and their agpaitic index (Fig. 2B, Table 6) is below 0.87 except for a few samples of Bessefjellet and Rustfjellet which lie between 0.87 and 1.00. This granitoid series is thus not alkaline (Liégeois, 1988). In the Peacock diagram (Fig. 2C), the overall trend is calc-alkaline and in the K_2O versus SiO_2 diagram of Peccerillo and Taylor (1976) (Fig. 2D), they plot in the high-K calc-alkaline and shoshonitic fields. Nevertheless, as these granitoids are also characterized by high FeOt/MgO, they plot in the tholeiitic field in the AFM diagram (Fig. 2E).

Besides their characteristic ferro-potassic geochemical signature, the granitoids have also A-type affinities. Indeed, they display high contents of Ga ($Ga/Al \times 10{,}000 > 2.6$: Whalen et al., 1987) and of incompatible elements ($Zr + Nb + Ce + Y > 350$ ppm: Whalen et al., 1987), relatively high alkali ($Na_2O + K_2O \sim 8$ wt.% at 70 wt.% SiO_2: Eby, 1990) and F contents (1126–6532 ppm). Originally defined by Loiselle and Wones (1979) (with the prefix A—standing for anorogenic, anhydrous and alkaline), the A-type definition has been revised later (e.g. Eby, 1990). The general consensus (e.g. Frost et al., 1999) is now to consider that the A-type granitoids emplace into non-compressive environments at the end of an orogenic cycle (postorogenic or postcollisional granitoids), in continental rift zones or in oceanic basins. Geochemically, they are characterized by low CaO and Al_2O_3, high FeOt/MgO, high K_2O/Na_2O and high incompatible elements contents. Moreover, A-type granites are commonly considered as being reduced (Loiselle and Wones, 1979) as clearly shown in the rapakivi-type subgroup (Emslie, 1991; Emslie and Stirling, 1993; Frost et al., 1999), but relatively oxidized A-type granites have also been recognized (i.e. Bogaerts et al., 2001; Dall'Agnol et al., 1999). The H_2O content of A-type granites is also a matter of discussion. These granites were originally thought as nearly anhydrous (Loiselle and Wones, 1979), but experimental data have clearly shown that they may contain several wt.% of H_2O (Bogaerts et al., 2001; Clemens et al., 1986; Dall'Agnol et al., 1999). Finally, A-type granites are not necessarily alkaline. Consequently, the A-type granites encompass a rather large group of rocks to which belongs the HBG suite.

6.2. The granitoids trend

6.2.1. Major elements

In Harker diagrams (Fig. 3), the nine intrusions define a single general trend with a small gap between 55

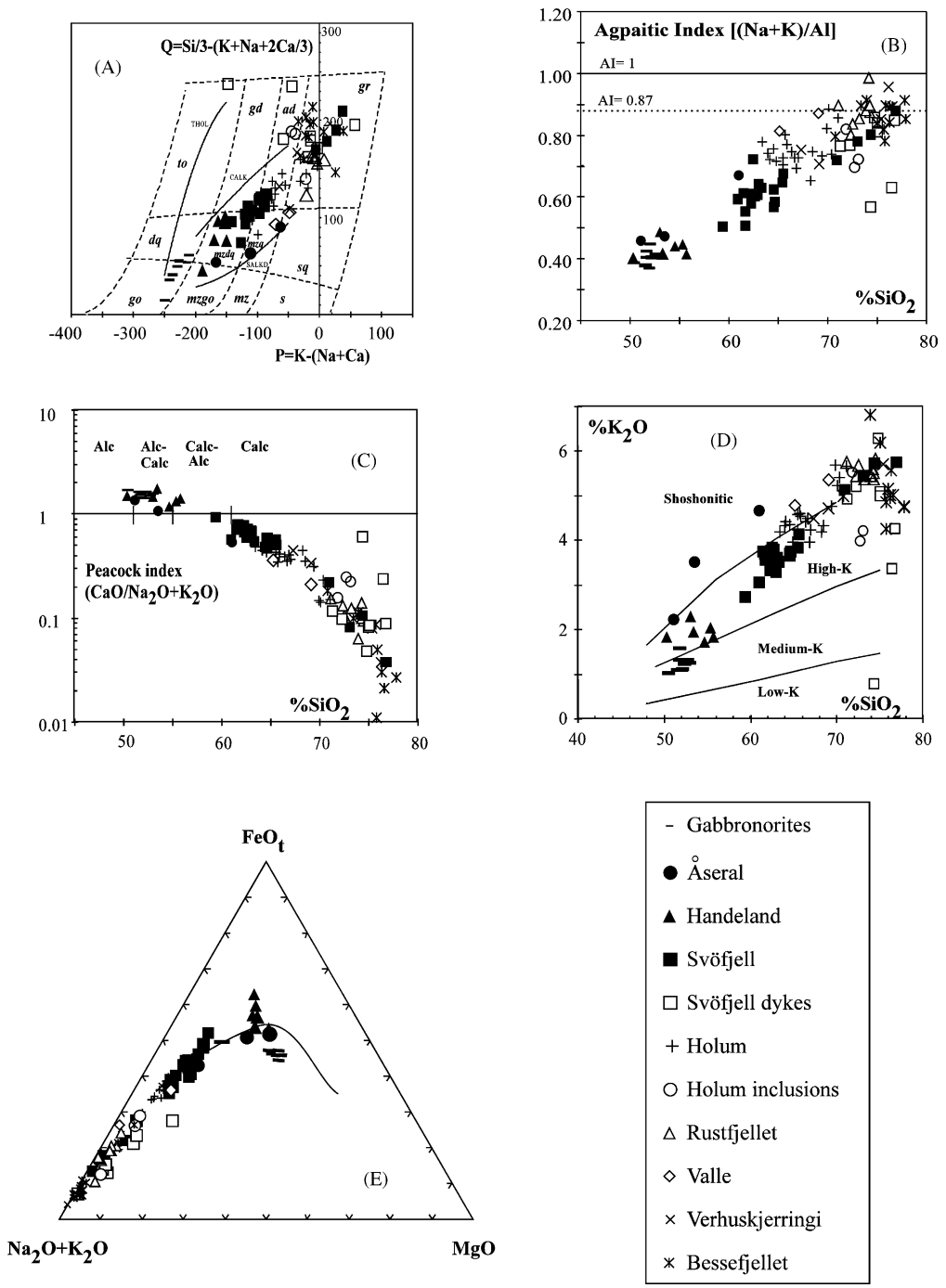

Fig. 2. Selected geochemical characteristics of the HBG suite. (A) Q = Si/3 − ((K + Na + 2Ca)/3) (at.%) vs. P = K − (Na + Ca) (at.%) of Debon and Le Fort (1983); (B) agpaitic index (Na + K)/Al (at.%) vs. SiO_2 (wt.%). The limit at AI = 0.87 is from Liégeois and Black (1987); (C) peacock index (CaO/(Na_2O+K_2O)) (wt.%) vs. SiO_2 (wt.%) after Brown (1981); (D) K_2O (wt.%) vs. SiO_2 (wt.%); the limits are from Rickwood (1989); (E) AFM diagram (wt.%); the limit between tholeiitic and calc-alkaline fields are from Irvine and Baragar (1971).

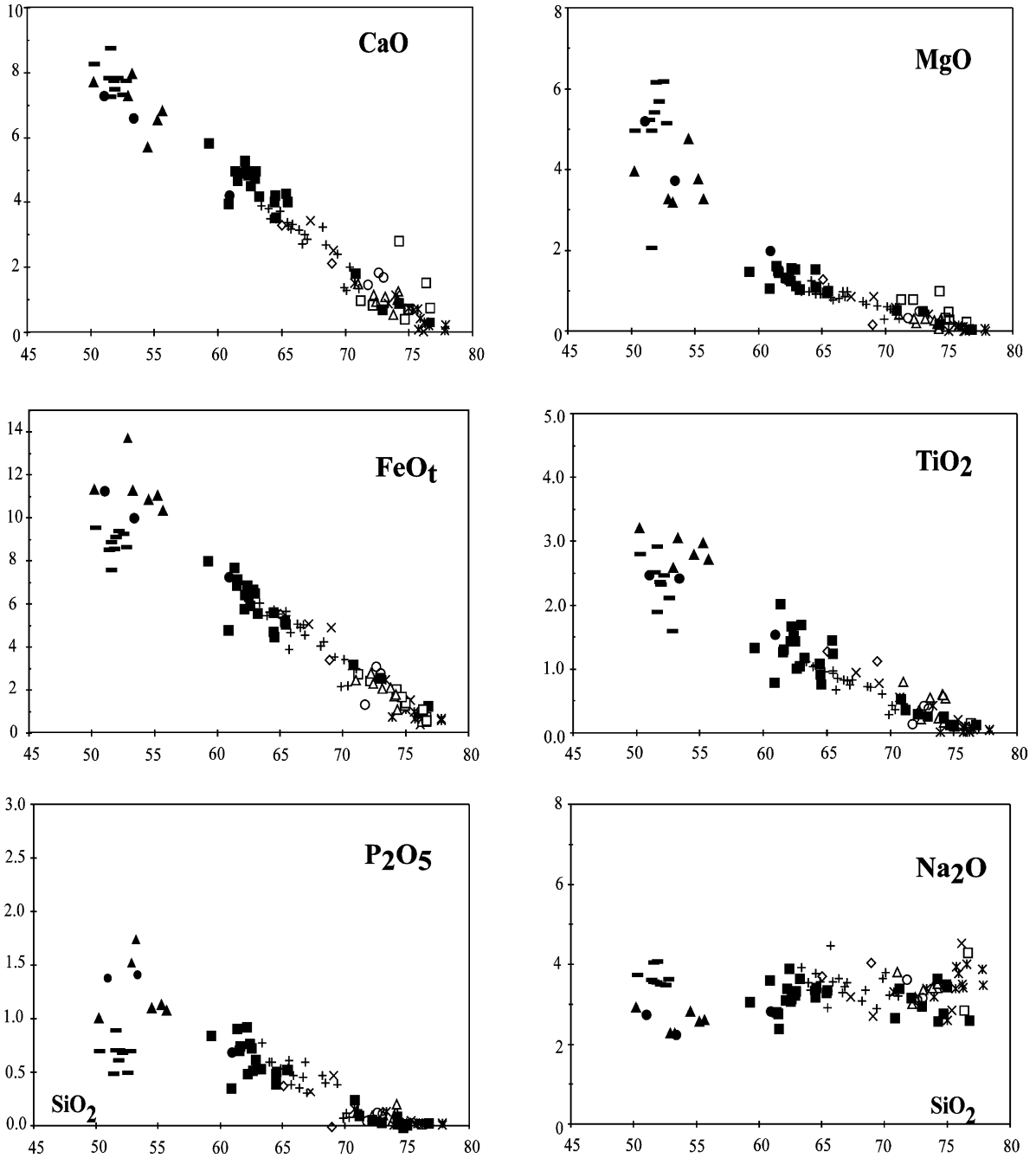

Fig. 3. Major elements content (wt.%) vs. wt.% SiO_2. Same symbols as in Fig. 2.

and 59 wt.% SiO_2. The latter could result from a lack of samples as mafic samples represent a very small proportion of the outcrops. Indeed, the three samples of the small Åseral intrusion plot on each side of the gap suggesting a possible continuity in the trend. There is some scatter in the data points (i.e. TiO_2 and P_2O_5 for Svöfjell) which probably results from samples not being representative of pure liquids but of crystal (ilmenite and/or apatite) laden liquids. With increasing SiO_2, there is a regular decrease in CaO, MgO, FeOt and TiO_2 from 55 wt.% SiO_2 whereas P_2O_5 first slightly increases and then decreases. A slight increase of FeOt and TiO_2 at low SiO_2 content is also observed. K_2O (see Fig. 2D) increases up to 72 wt.% SiO_2 and then decreases. Na_2O remains relatively constant with increasing SiO_2 whereas Al_2O_3 (not shown) slightly decreases in the gabbronorites and then remains constant in granitoids.

6.2.2. Trace elements

Sr, Zr, Ba, Ce (not shown), Y, Nb and Sc display a bell-shape trend with increasing SiO_2, whereas Co and V (not shown) regularly decrease and Rb increases (Fig. 4). The high Zr contents (900 up to 1100 ppm) observed in several samples of Holum likely results from some accumulation of zircon. Nb behaves similarly to Zr, as commonly observed (e.g. Duchesne and Wilmart, 1997), except in Bessefjellet where the amplitude of the variation is an order of magnitude larger than in the general trend.

REE patterns of selected samples from the different massifs and corresponding to various SiO_2 contents are shown in Fig. 5. The various patterns differ by the $(La/Sm)_N$ ratios and the magnitude of the Eu anomaly, and might correspond to different degrees of differentiation (see below for a discussion about the possible differentiation processes). The REE content first increases from the gabbronorites to sample 98BN41C of Holum and the least differentiated sample of the Svöfjell massif. Then the REE content decreases down to sample BE6 where a strong increase in the $(La/Sm)_N$ is observed. The Eu anomaly is first absent (Sk9, A10), then slightly positive (98BN39A) or, more frequently, slightly negative (SV90-13, 98BN41C, R7, H14). Finally, a strong negative Eu anomaly is displayed in samples BE4, BE5 and BE6. The average $(La/Yb)_N$ ratio (see Table 6) is higher in Rustfjellet (36.2) and Valle (40.2) than in the main granite of Svöfjell (7.6), Vehuskjerringi (7.8) and Bessefjellet (7.6). On the other hand, the gabbronorite is characterized by small $(La/Yb)_N$ values (average of 7.39: Demaiffe et al., 1990).

The N-MORB-normalized spidergrams of the average composition of the different massifs are shown in Fig. 6. These patterns are characterized by negative anomalies in Ba, Nb, Ta, Sr, P and Ti. The negative anomalies in Ba, Sr, P and Ti are more or less pronounced, consistent with different degrees of differentiation in the selected samples.

6.2.3. Isotopic data

Sr and Nd isotopic data are presented in Table 7 together with data from various typical gneisses. All calculations have been performed following Ludwig (2001), implying that errors were multiplied by $\sqrt{}$MSWD when the latter was >1.2. The ages and thus initial isotopic compositions are known for the gabbronorites and some of the selected granitoids: gabbronorites (910 ± 82 Ma (Rb-Sr), $I_{Sr(930\,Ma)} = 0.7052–0.7054$, $\varepsilon_{Nd(930\,Ma)} = +0.4$ to $+1.97$, $^{206}Pb/^{204}Pb = 17.45$, $^{207}Pb/^{204}Pb = 15.51$: Demaiffe et al., 1990), Verhuskjerringi (932 Ma: U/Pb, Dahlgren, personal communication in Sylvester, 1998) and Bessefjellet (923 ± 16 Ma (Rb/Sr): Killeen and Heier, 1975). Enough samples have been measured on the Holum pluton for geochronological purposes and an age indication of 929 ± 47 Ma is obtained ($Sr_i = 0.7046 \pm 0.0006$, MSWD = 1.7 for 7 WR; Fig. 7). An older age of 980±34 Ma was proposed by Wilson et al. (1977) for this intrusion but if errors are considered, both ages overlap. When all measured HBG samples are considered, including samples from the Lyngdal massif (Bogaerts et al., in press), an errorchron is obtained but with a reasonable MSWD for such a large number of samples collected in a series of plutons extending along a distance of more than 100 km: 965 ± 19 Ma, $Sr_i = 0.70433 \pm 0.00056$, MSWD = 14 for 39 WR (Fig. 7). When samples of the Bessefjellet pluton are excluded from the errorchron as their very high Rb/Sr could impose the slope, results are similar: 957 ± 25 Ma, $Sr_i = 0.70447 \pm 0.00064$, MSWD = 15 for 37 WR (Fig. 7). These ages are identical within error limits, the weighted average being: 961 ± 14 Ma with a MSWD = 0.97. This latter value gives more weight to the individual pluton ages than the former one and initial ratios are also nearly identical. Based

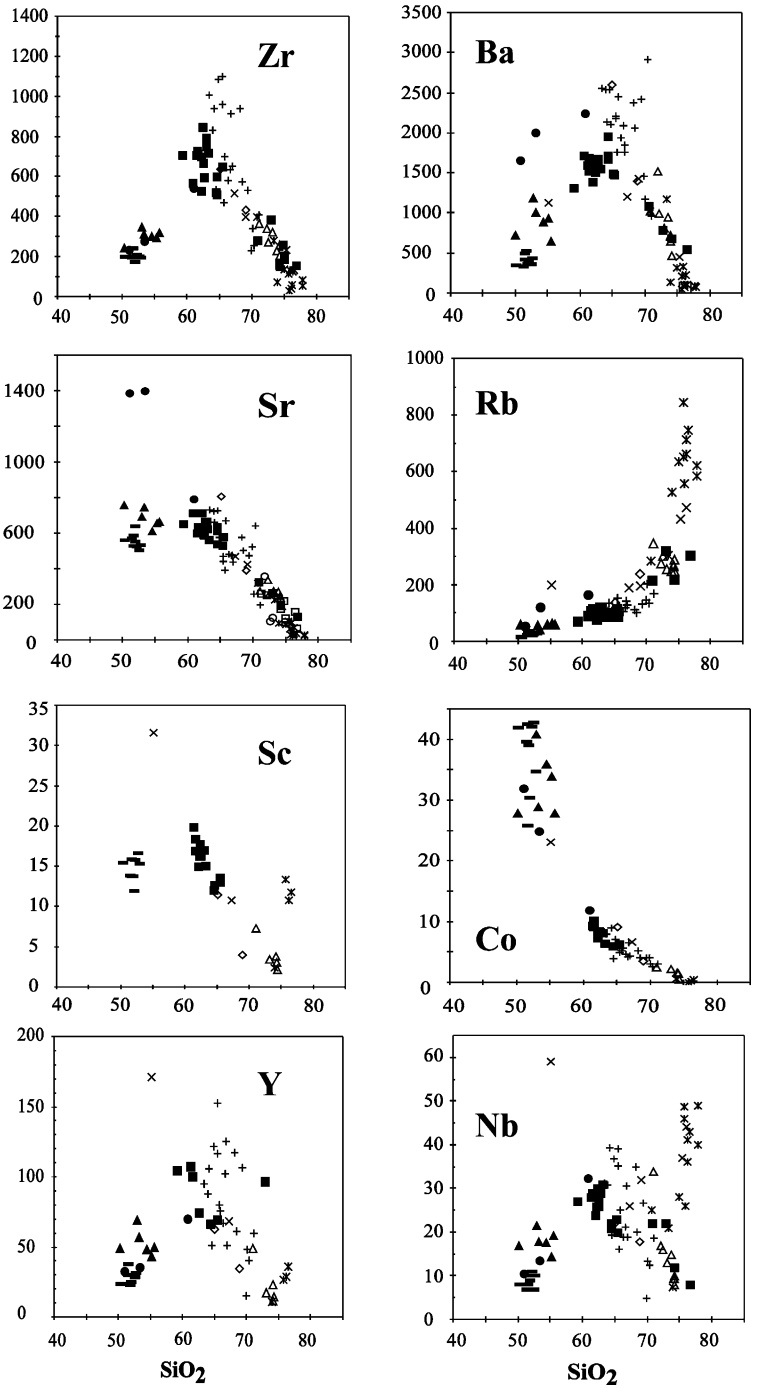

Fig. 4. Trace elements content (ppm) vs. wt.% SiO_2. Same symbols as in Fig. 2.

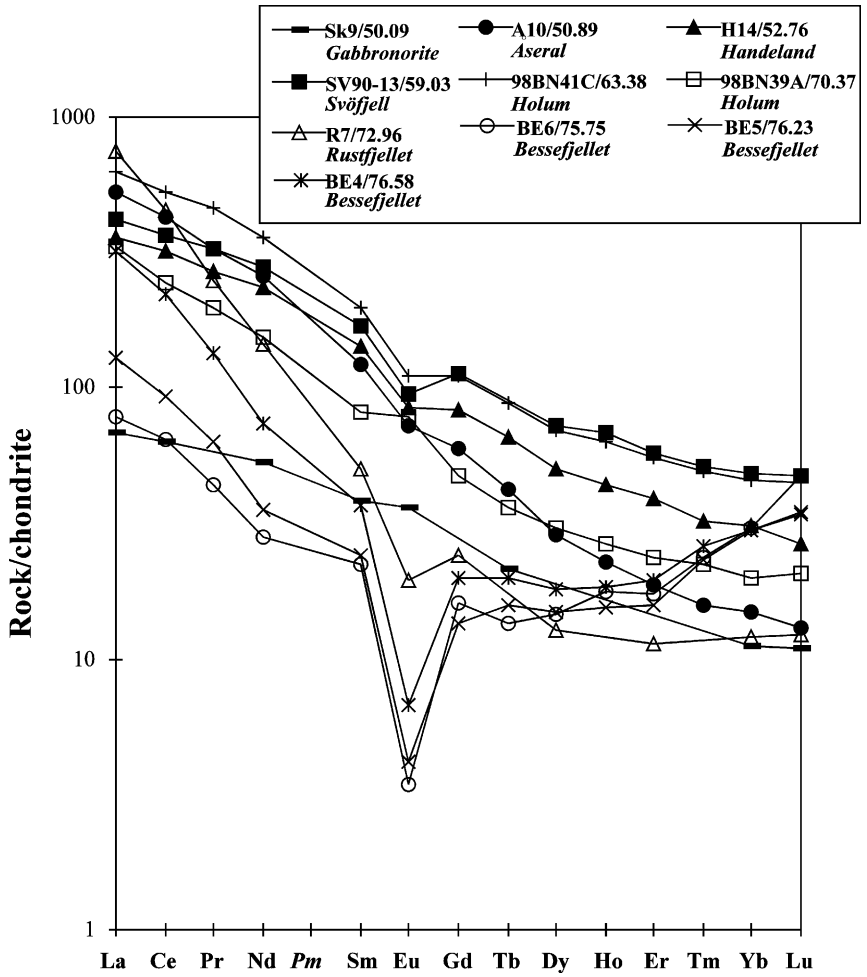

Fig. 5. Chondrite-normalized REE patterns. Chondrite values from Sun and McDonough (1989). Values on the right of sample numbers correspond to wt.% SiO_2.

mainly on errorchrons, these ages are not geologically entirely meaningful but are in agreement with the U-Pb zircon age of 950 ± 5 Ma on the Lyngdal massif (Pasteels et al., 1979). However, the actual time span during which the HBG suite emplaced is not precisely constrained. For instance, the Holum massif (929 ± 47 Ma) and the small Verhuskjerringi massif could be younger than 961 Ma if the cf. 932 Ma U-Pb zircon age for this latter massif is confirmed (Dahlgren, personal communication in Sylvester, 1998). Moreover, at 961 Ma, the I_{Sr} of the Rustfjellet pluton is unrealistically low (0.7011–0.7015; Table 7). Consequently, I_{Sr} and ε_{Nd} have been calculated at 930 Ma, the emplacement age of the Rogaland AMC suite (Schärer et al., 1996). Note that recalculating the initial ratios at 961 Ma would not change the results much except for samples with very high Rb/Sr ratios but for these samples, the error on their initial ratios (Table 7) is so high that they are not very useful. At 930 Ma (Fig. 8), the granitoids display a characteristic narrow range in I_{Sr} from 0.7027 (R7) up to 0.7056 (SV6) and a larger range in $\varepsilon_{Nd(t)}$ (+2.0: Sk10: Demaiffe et al., 1990 down to −4.9 (VA2)). In Bessefjellet, the $^{87}Rb/^{86}Sr$ ratio is relatively high (62–66, Table 7) implying that the calculated I_{sr} is rather imprecise and strongly age dependent (at

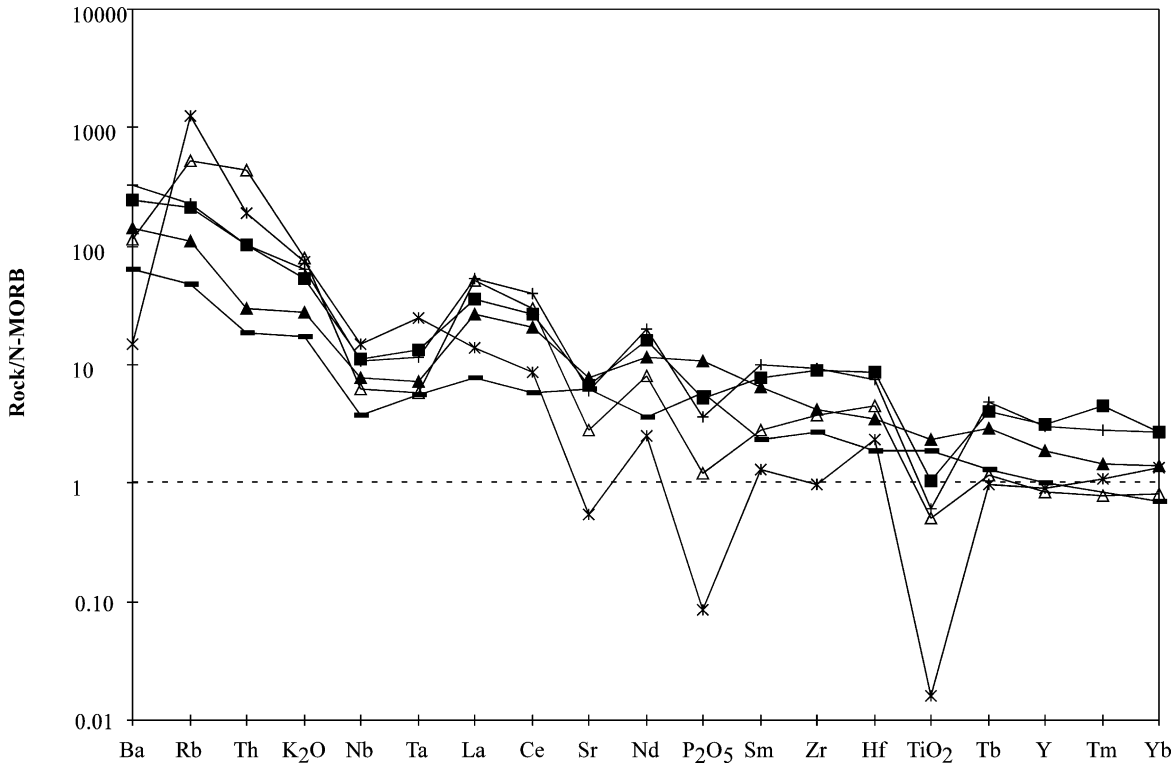

Fig. 6. N-MORB normalized spidergrams of average compositions. N-MORB values from Sun and McDonough (1989). Same symbols as in Fig. 2.

930 Ma, I_{sr} = 0.7329–0.7569 and $\varepsilon_{Nd(t)}$ = −6.5 and −3.9). Data for the Herefoss granite (Andersen, 1997) have also been plotted in Fig. 8 and fall in the range of the granitoids studied here. Our data are also in agreement with results of Andersen et al. (2001). The intrusions of Svöfjell, Rustfjellet, Valle, Verhuskjerringi and Holum have Sr contents higher than 150 ppm, $^{87}Rb/^{86}Sr$ ratio <5, $I_{sr} < 0.710$ and $\varepsilon_{Nd(t)} < 0$, they thus belong to the 'normal Sr concentration granite' of Andersen et al. (2001). Bessefjellet has a Sr content lower than 150 ppm, a $^{87}Rb/^{86}Sr$ ratio >5, $I_{sr} > 0.710$ and $\varepsilon_{Nd(t)} < 0$ and thus fall in the 'low Sr granite' group of the same authors, the gabbronorites have an $I_{sr} < 0.705$ and $\varepsilon_{Nd(t)} > 0$.

Model ages have been calculated according to the depleted mantle model of Nelson and DePaolo (1984) and are shown in Table 7. They range from 1.4 to 1.7 Ga (plus sample BE5 at 2.2 Ga) and are in agreement with model ages presented by Andersen et al. (2001).

The two samples collected close to Svöfjell (84-48: charnockitic dyke and 84-53: granite) have clearly distinct I_{sr}, 0.7168 and 0.7075, respectively; they are quite different from Svöfjell (I_{Sr} = 0.7039 to 0.7049) and are thus not comagmatic with this body.

7. Geothermobarometry

Several granitoids contain the appropriate assemblage (plagioclase, K-feldspar, quartz, ilmenite or magnetite, titanite, hornblende and biotite) to use the Al-in-hornblende geobarometer. We have used the two experimental calibrations of this geobarometer (fluid-saturated with varying proportion of H_2O and CO_2: Johnson and Rutherford, 1989; H_2O-saturated fluid: Schmidt, 1992) as well as the Anderson and Smith (1995) calibration which incorporates temperature as well as the above-mentioned experimental data. For this latter calibration, temperature was

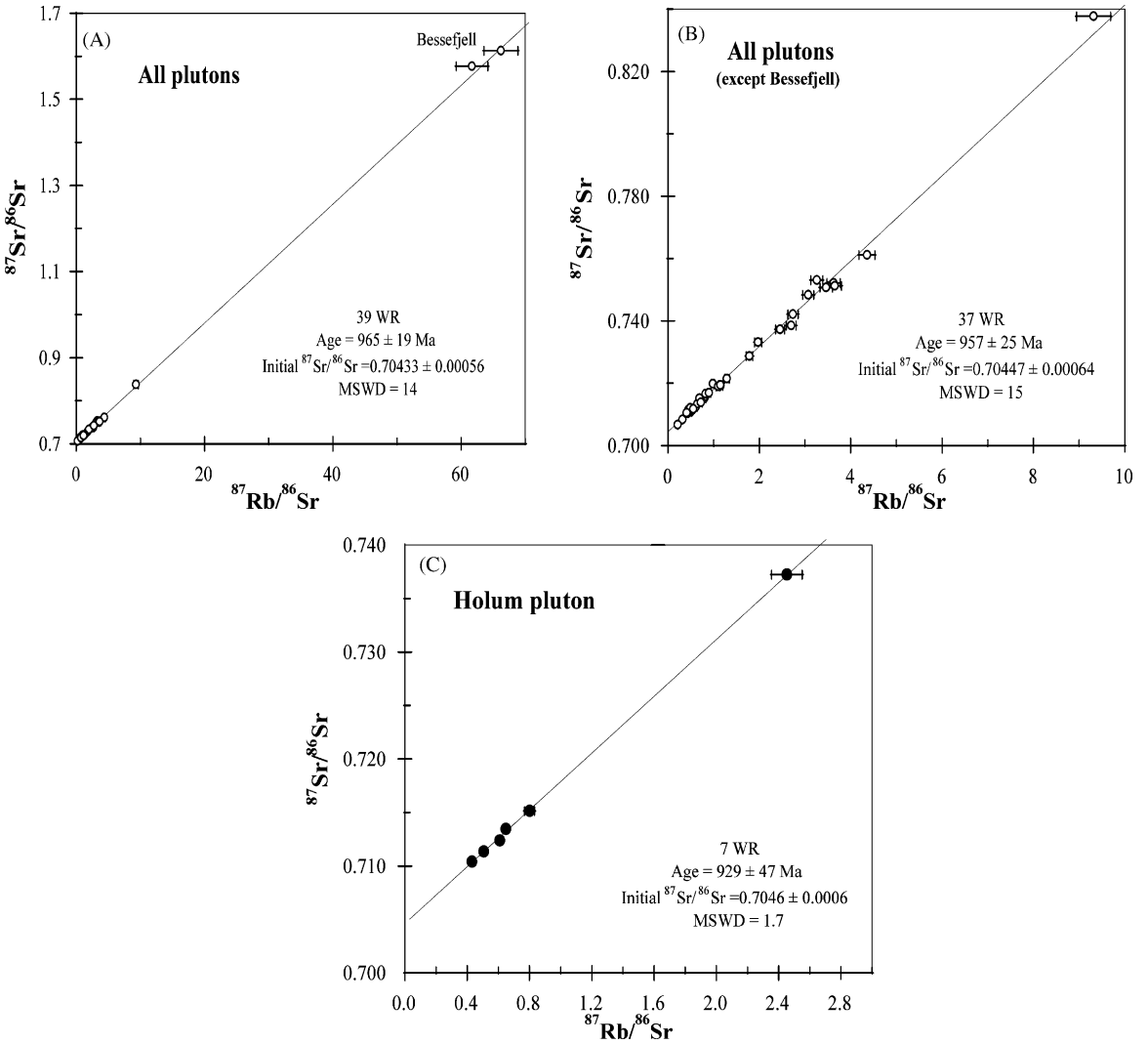

Fig. 7. Rb-Sr plots of all plutons (A), all plutons except Bessefjellet (B) and Holum (C).

estimated with the hornblende-plagioclase thermometer of Holland and Blundy (1994), in which amphibole composition was recalculated according to the formula embedded in this thermometer. Results (Table 8) indicate a pressure range from 1.3 up to 5.6 kb. When temperature is taken into account, the pressure range is reduced to 1.3 up to 2.7 kbar (Anderson, 1996). These granitoids appear thus to be rather low pressure plutons; it is important to keep in mind however that a pressure of 2 kbar is the lower limit of the calibration range of the geobarometer. Nevertheless, these pressure estimates are in agreement with recent experimental data obtained on the Lyngdal granodiorite which belongs to the HBG suite (Bogaerts et al., 2001). The calculated pressure range for the HBG suite overlaps the pressure of emplacement of the Rogaland AMC suite ($\leq$5 kbar: Vander Auwera and Longhi, 1994; Vander Auwera et al., 1998a) suggesting that both suites were emplaced approximately at the same level of the upper crust and maybe at the same age ($\approx$930 Ma) (Schärer et al., 1996).

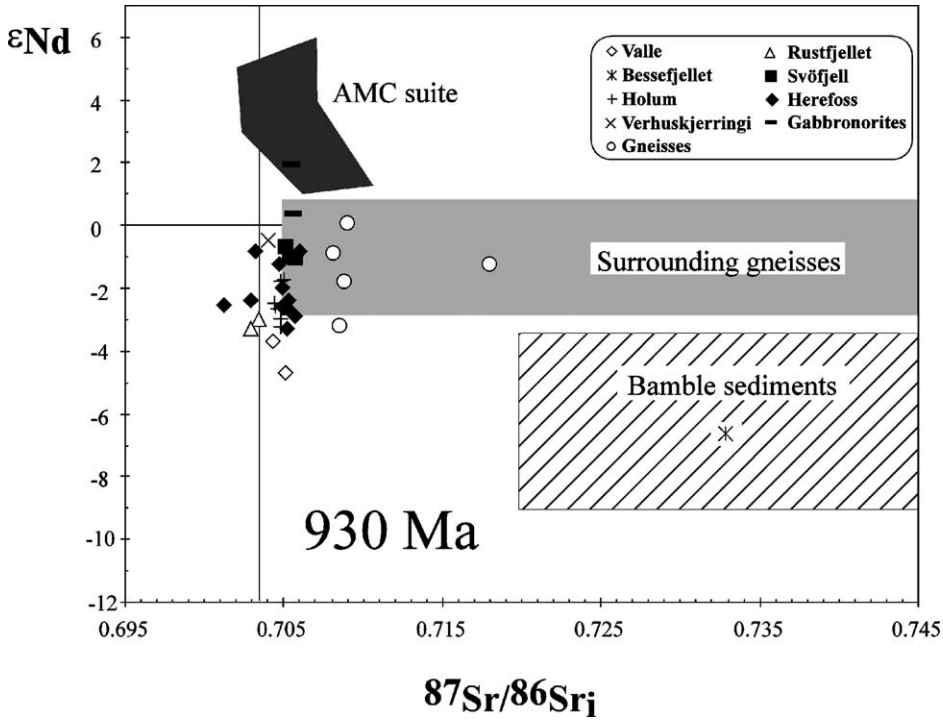

Fig. 8. ε_{Nd} vs. I_{Sr} for the HBG suite calculated back at 930 Ma. Data: Herefoss from Andersen (1997), gabbronorites from Demaiffe et al. (1990), surrounding gneisses from Demaiffe et al. (1986), Menuge (1982) and Menuge (1988), Bamble sediments from Andersen et al. (1995), and AMC suite from Demaiffe et al. (1986).

Several geothermometers have been used to estimate temperatures of crystallization. Temperatures estimated with the hornblende-plagioclase geothermometer of Holland and Blundy (1994) range between 798 and 825 °C and the hornblende-clinopyroxene equilibrium (Perchuk et al., 1985) gives a temperature of 770 °C for sample SV90-13.

The equations derived from the experimental data of Harrison and Watson (1984) and Watson and Harrison (1983) on the solubility of zircon and apatite in subaluminous melts can be used as geothermometers. Results are shown in Table 8: apatite saturation temperatures range from 1005 up to 1054 °C whereas zircon saturation temperatures are much lower (774

Table 8
Results from geothermobarometry

	VA1	S2	SV6	SV90-13
P (kbar): Al-in-hornblende				
Johnson and Rutherford (1989)	4.3	2.5	3.5	3.5
Schmidt (1992)	5.6	3.6	4.6	4.9
Anderson and Smith (1995)	2.5	1.3	2.2	2.7
T (°C)				
Hornblende-plagioclase (Holland and Blundy, 1994)	825	810	808	798
Hornblende-clinopyroxene (Perchuk et al., 1985)				770
Zircon (Watson and Harrison, 1983)	863	774	876	870
Apatite (Harrison and Watson, 1984)	1005	1125	1053	1054

to 876 °C). Temperatures obtained with these geothermometers agree with petrographic and chemical data. For example, in sample SV90-13 (Svöfjell) apatite occurs as small needles dispersed in the other phases, suggesting its early crystallization and thus the presence of apatite at or near the liquidus of the magma. From the P_2O_5–SiO_2 diagram, it can be deduced that apatite saturation occurred around 53 wt.% SiO_2. On the other hand, the low temperatures of zircon saturation are similar to those obtained for amphibole crystallization and the occurrence of rims of hornblende surrounding clinopyroxene supports their late crystallization. Moreover, this hypothesis is corroborated by the bell-shape trend observed in the Zr versus SiO_2 diagram (see Fig. 4) pointing to zircon saturation at 63 wt.% SiO_2. These data thus show that several phases occurring in a single sample did not necessarily crystallize simultaneously and further indicate that the mineral composition may register intervals of equilibrium crystallization.

The assemblage magnetite + quartz + titanite in the granitoids suite suggests an oxygen fugacity above NNO (Wones, 1989).

8. Discussion

8.1. Possible differentiation processes

In Harker diagrams, the small intrusions of Åseral, Handeland-Tveit as well as the Lyngdal and Skoland gabbronorites plot on the same trend as the larger granitoids (Figs. 3 and 4) suggesting that they all belong to the same suite of rocks. The Lyngdal and Skoland gabbronorites were previously thought to belong to the AMC suite (Demaiffe et al., 1990) as they display similar mineralogical and geochemical compositions to the jotunites (hypersthene bearing monzodiorites) of this latter suite. The gabbronorites and jotunites show comparable enrichments in TiO_2, P_2O_5, K_2O as well as similar REE patterns and isotopic data suggest that they derive from the same isotopic reservoir (Demaiffe et al., 1990). Nevertheless, significant mineralogical and geochemical differences do also occur. Biotite is a late stage phase in both gabbronorites and jotunites but it is much more abundant in the former rocks suggesting that these contain a few wt.% of H_2O, whereas the jotunites are practically anhydrous. The gabbronorites are distinctly lower in (Na + K)/Al (agpaitic index) and FeOt and higher in CaO than jotunites, and in most variation diagrams, the AMC and HBG (including the gabbronorites) suites define two distinct trends (Vander Auwera et al., 2001; Vander Auwera et al., in preparation). It is also worth emphasizing that the Lyngdal and Skoland gabbronorites outcrop at the northern margin of the Lyngdal granodiorite, which is the southernmost HBG pluton of the Rogaland-Vest Agder sector (Bogaerts et al., in press) (Fig. 1), and, in this massif, lobate enclaves of gabbronorites are mingled with the granodiorite clearly indicating that both rock types are representative of penecontemporaneous liquids and are thus genetically linked. The relic cores of clinopyroxenes observed in some amphiboles of Svöfjell (see Table 5) have a Mg# of 0.66. Using the Fe-Mg exchange distribution coefficient of 0.23 (Grove and Bryan, 1983), the calculated Mg# of the liquid in equilibrium with these clinopyroxenes is 0.31. This value is lower than the Mg# of the gabbronorites (≈0.5), but higher than the Mg# of the least differentiated sample of Svöfjell (Mg# = 0.25). Moreover, the relic cores of clinopyroxene have certainly not retained their liquidus composition as they reacted to amphiboles: their Mg# is thus a minimum value. As discussed above, the gap occurring between 55 and 59 wt.% SiO_2 probably results from the small proportion of mafic samples as the higher density of these magmas traps them in the lower crust and/or from the fact that they have differentiated to produce more evolved magmas plus cumulates. Moreover, as already mentioned, the three samples of the Åseral intrusion plotting on each side of the gap give further support to a continuous trend.

The trend ranging from 50 up to 78 wt.% SiO_2 defined by the HBG suite could result from mixing processes between two (basaltic and granitic) or three (basaltic, intermediate and granitic) components, from partial melting processes or from a fractional crystallization process with (AFC process) or without assimilation. Mixing between two components can be precluded here. It should result in linear evolution in all variation diagrams, which is obviously not the case here. Indeed, several elements (P_2O_5, Zr, Ba, Sr and Sc: Figs. 3 and 4) show a bell-shape evolution indicating that with increasing content of an incompatible element, the liquid becomes saturated in a phase containing the element (which therefore

becomes compatible): apatite for P_2O_5, zircon for Zr (see above discussion), biotite for Ba, plagioclase for Sr, and in the case of Sc, zircon, ilmenite, cpx, opx and magnetite are possible (Mahood and Hildreth, 1983). The presence of these bell-shape curves thus supports a fractional crystallization process. However, these trends could also result from two mixing stages between three components: a first mixing stage between the gabbronorites and an intermediate component similar in composition to the least differentiated sample of Svöfjell (e.g. SV90-13: see Table 6) and a second mixing stage between the intermediate and the granitic components. This hypothesis is however unlikely for four reasons: (1) when mixing occurs between more than two components, representative samples are usually much more dispersed in Harker diagrams and particularly occur inside the concavity of the bell-shape curves (see the example of the Tismana pluton: Duchesne et al., 1998); (2) a Rb-Sr isochron has been obtained for Holum which makes mixing between the intermediate and granitic components unlikely; (3) the first mixing stage should have produced linear arrays in all variation diagrams which is not the case here as TiO_2, P_2O_5 and FeOt display a slight increase and then a steady decrease with increasing SiO_2 (Fig. 3); (4) the isotopic composition of the gabbronorites ($I_{Sr} = 0.7052$–0.7054, $\varepsilon_{Nd(t)} = +0.4$ to $+1.97$: Demaiffe et al., 1990) is close to that of the less contaminated granitoid (Verhuskjerringi: $I_{Sr} = 0.70385$; $\varepsilon_{Nd(t)} = -0.68$: Table 7 and Fig. 8). One could further argue that the lack of samples inside the concavity of the bell-shape curves in Harker diagrams is not a definitive argument as the two stages of the mixing process could have occurred at two different crustal levels, in successive magma chambers at decreasing depths. Nevertheless, representative samples of this supposed first mixing stage (that took place at a lower crustal level), were finally emplaced in the upper crust where they should have been mixed with the granitic end-member, hence producing samples plotting inside the concavity of the bell-shape curves. Moreover, such a two-stage mixing process does not encounter the other arguments: isochron obtained for Holum; non-linear arrays in the TiO_2, P_2O_5 and FeOt variation diagrams. In conclusion, even if rather complex mixing processes occurring in separate systems cannot be completely ruled out here, we suspect that they would have produced much more scatter in the variation diagrams and we thus not retain a mixing process to explain the observed trend. The lobate inclusions of gabbronorites observed in the Lyngdal granodiorite are thus interpreted as mafic injections in a more differentiated, still partially liquid magma chamber.

Two melting processes of two different protoliths could produce a broken linear array. Nevertheless, it is shown by Bogaerts et al. (in press) that a melting process does not fit the representative data points of the Lyngdal granodiorite (very similar to Svöfjell) which corresponds to the second part of the HBG trend. On the contrary, a fractional crystallization process is successfully modelled for major and trace elements using the least squares regression method and experimental data (Bogaerts et al., 2001). The fractionating cumulate is made of clinopyroxene, hornblende, plagioclase, oxides, biotite, apatite, zircon and allanite (Bogaerts et al., in press). A melting process could indeed explain the first part of the HBG trend but this hypothesis implies that the second part of the trend would correspond to the fractional crystallization of the low degree melts of this first melting process. A question thus remains open: why the other liquids of this melting process did not evolve through fractional crystallization? Other observations do not favor this melting process. The three data points of the Åseral intrusion straddle the two parts of the HBG trend (see Co versus SiO_2 in Fig. 4) pointing to an identical differentiation process, fractional crystallization, for both parts of this trend. The Rb-Sr isochron (910 ± 82 Ma, MSWD $= 0.74$) obtained by Demaiffe et al. (1990) on the gabbronorites is also better explained by a fractional crystallization process. Finally, in a bilogarithmic Co (compatible element) versus Rb (strongly incompatible element) plot (Fig. 9) (Allègre et al., 1977; Hanson, 1978), the HBG trend can be approximated by a broken line supporting the hypothesis of a fractional crystallization process. The first segment of this line includes the Handeland-Tveit intrusion and two samples of Åseral and the second, the rest of the samples. These two segments could correspond to the subtraction of two distinct cumulates (Allègre et al., 1977), in agreement with observations from variation diagrams.

We thus conclude that the observed HBG trend results from a fractional crystallization process in which granitic compositions are derived by extensive fractionation of several batches of basic magmas

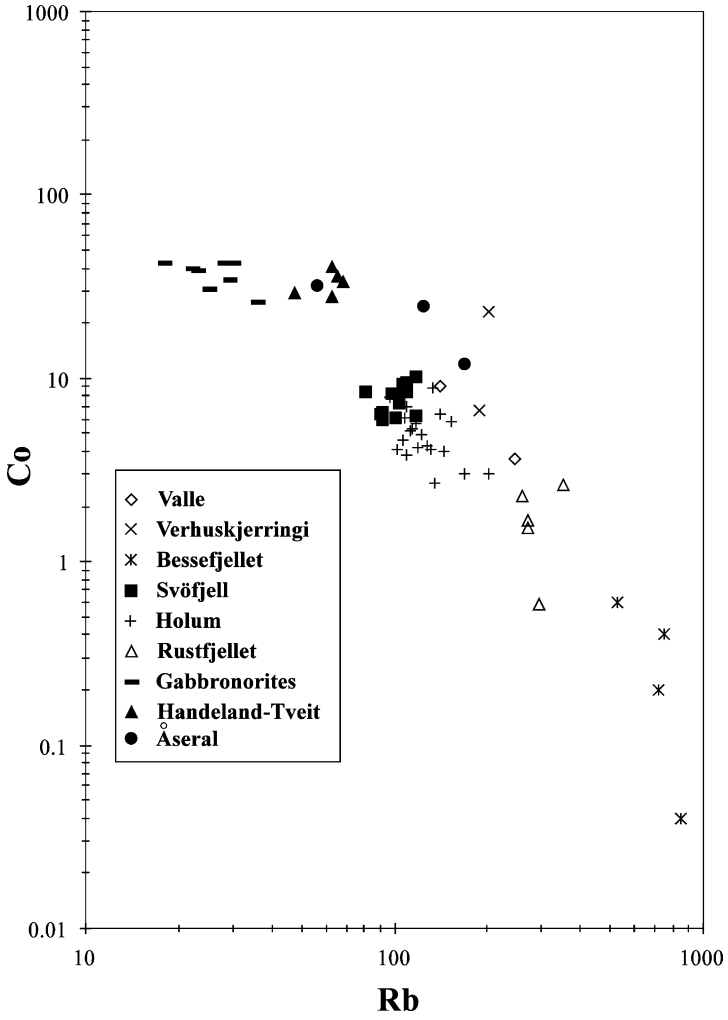

Fig. 9. Co and Rb (ppm) contents in bilogarithmic scale.

having similar major and trace elements compositions. This hypothesis of extensive fractional crystallization of basalts to produce A-type granites was already pointed out by Frost and Frost (1997), Loiselle and Wones (1979) and Turner et al. (1992). Cumulates formed during this fractional crystallization process were probably trapped lower in the crust as no layered intrusion belonging to the HBG suite has ever been observed at the present level of exposure. It is worth noting that in the penecontemporaneous AMC suite the whole series of corresponding cumulates has been described in the Bjerkreim-Sokndal layered intrusion (Wilson et al., 1996).

The narrow range of I_{sr}, the existence of reliable Rb-Sr age indications together with a quite large variation in ε_{Nd} (+1.9 to −6.51) in the members of the HBG suite can result either from sources with variable ε_{Nd} or from assimilation during fractional crystallization (AFC process), the two processes may have played a role together. The two gabbronorites have similar SiO_2 content but very different ε_{Nd} (Sk10: +1.9 for 51.38 wt.% SiO_2; Ly11a: +0.4 for 51.62 wt.% SiO_2: Demaiffe et al., 1990) indeed suggesting source variability. Andersen et al. (2001) noted that for most granites, the depleted mantle Nd model ages (T_{DM}: 1.38–1.67 Ga) decrease slightly westwards from the

Østfold-Akershus sector to the Rogaland-Vest Agder sector. They attributed this slight decrease to a progressive increase of the proportion of juvenile component in the source of the granitic magmas. In this latter model, the T_{DM} model ages are intermediate between the ages of the two possible components (juvenile and crustal) of the source, indicating an old crustal contaminant at least older than 1.67 Ga, possibly of Svecofennian age (cf. 2 Ga). In the hypothesis of an AFC process, the banded gneisses sampled in the vicinity of the plutons (Tables 6 and 7) and at some distance from the Rogaland anorthositic complex as well as the Bamble metasediments (Andersen et al., 1995) have too high I_{Sr} and ε_{Nd} to be plausible contaminants. Isotopic data favor contamination by a Rb-depleted material characterized by strongly negative ε_{Nd} and intermediate I_{sr} (<0.710), i.e. an old granulitic lower crust.

8.2. Non-CHARAC or/and tetrad effects

The Bessefjellet intrusion displays geochemical characteristics significantly different from those of the other intrusions: high Rb/Sr ratio (Table 6), low K/Rb ratio, almost vertical trends in the Rb versus SiO_2, Nb versus SiO_2 (Fig. 4) and Ta versus SiO_2 (not shown) plots. Moreover, some samples have a peraluminous character. The Rb and Nb vertical trends are difficult to ascribe to magmatic differentiation; fluid/rock interaction (non-CHARAC or tetrade effects) at the magmatic stage can be suspected. In a geochemical system characterized by charge-and-radius-controlled (CHARAC) trace elements behaviour, elements having close charges and radii are expected to show coherent behavior (chondritic ratios) and normalized patterns of the trivalent REE should be smooth

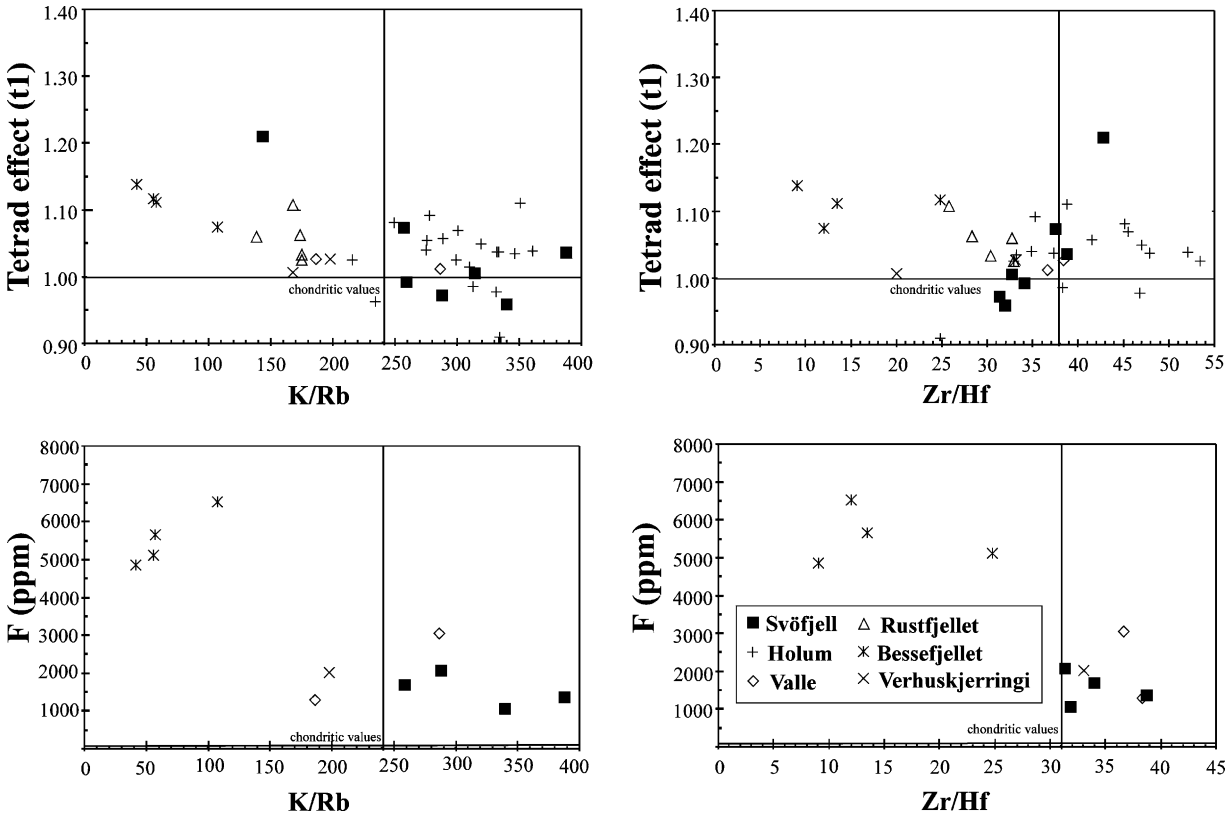

Fig. 10. Tetrad effect (t1 parameter from Irber, 1999: $TE_{1,3} = (t1 \times t3)^{0.5}$; $t1 = (Ce/Ce^t \times Pr/Pr^t)^{0.5}$ with $Ce/Ce^t = Ce_N/(La_N^{2/3} \times Nd_N^{1/3})$ and $Pr/Pr^t = Pr_N/(La_N^{1/3} \times Nd_N^{2/3})$; $t3 = (Tb/Tb^t \times Dy/Dy^t)^{0.5}$ with $Tb/Tb^t = Tb_N/(Gd_N^{2/3} \times Ho_N^{1/3})$ and $Dy/Dy^t = Dy_N/(Gd_N^{1/3} \times Ho_N^{2/3})$ vs. K/Rb and Zr/Hf and F content (ppm) versus K/Rb and Zr/Hf. Chondritic values are from Anders and Grevesse (1989). See text for explanation.

functions of atomic number and radius (Bau, 1996; Jahn et al., 2001). Highly evolved magmas, like Bessefjellet, are potentially very enriched in H_2O, F, P, Cl and appear therefore transitional between pure silicate melts and hydrothermal fluids. In such systems, the behavior of trace elements can also be governed by complexation processes resulting in non-chondritic Y/Ho, Zr/Hf ratios or even in the lanthanide tetrad effect (Bau, 1996; Jahn et al., 2001). The tetrad effect refers to the subdivision of the REE into four groups called tetrads (La-Nd, Pm-Gd, Gd-Ho, Er-Lu) displaying upwards or downwards concavities with minima at La, between Nd and Pm, at Gd, between Ho and Er, and at Lu (Bau, 1996; Irber, 1999). In order to quantify the tetrad effect, Irber (1999) has proposed to use the $TE_{1,3}$ ($=(t1 \times t3)^{0.5}$) parameter (see Fig. 10) which determines the deviation of a REE pattern with a tetrad effect from a hypothetical effect-free REE pattern. We have used here only the t1 parameter which evaluates this deviation for the first tetrad (La to Nd) as the third tetrad (Gd to Ho) does not show any concavity ($t3 = 1$) (Fig. 5). In Fig. 10, the tetrad effect t1 parameter of Irber (1999) and the F content are shown as function of the K/Rb and Zr/Hf ratios and compared with the chondritic values of these parameters. Fig. 10 shows that in Bessefjellet, a very slight tetrad effect is significant (above 1.1: Irber, 1999) only in three samples. Nevertheless, the K/Rb, Zr/Hf and Nb/Ta ratios (not shown: average of 11 in Bessefjellet compared to 17 for the chondritic value) are indeed much lower than chondritic values and are correlated with high F contents in this intrusion.

9. Possible sources and geodynamic implications

In order to better constrain the geodynamical setting of the HBG suite, the possible sources of the parent gabbroic magmas have to be discussed. We have mentioned above that the magmas that gave rise to the gabbronorites of the HBG suite probably contained several percent H_2O. This moderate H_2O content must be ultimately derived from the source which contained hydrated phases (e.g. mica, amphibole). Moreover, the gabbronorites are characterized by low $(La/Yb)_N$ values (average of 7.39: Demaiffe et al., 1990) suggesting that garnet was absent in the residue. It is thus plausible that these gabbronorites were derived by partial melting of a garnet-free, hydrated, undepleted to slightly depleted ($\varepsilon_{Nd} > 0$) and potassic mafic source, lying either in the lithospheric upper mantle or in the mafic lower crust derived from it. It is worth mentioning here that experimental data obtained by Rapp and Watson (1995) on dehydration melting of metabasalts are in agreement with this hypothesis. Experimental liquids obtained at 8 kbar and 1075, 1050 and 1000 °C from an amphibolite are very similar in composition to the gabbronorites and the Handeland small intrusion of the HBG suite (Vander Auwera et al., in preparation).

As already mentioned above, the HBG suite is close in age and space with the AMC suite of Rogaland (≈930 Ma). The parent magmas of this suite are the least differentiated jotunites (Demaiffe and Hertogen, 1981; Duchesne et al., 1974; Vander Auwera et al., 1998a), called primitive jotunites by Vander Auwera et al. (1998a), and phase equilibria based on experimental data further indicate that these primitive jotunites are products of the partial melting of an anhydrous gabbronorite source (mafic granulite or gabbronoritic cumulates) in the lower crust (11 kbar) (Longhi et al., 1999). Consequently, partial melting of two distinct sources (a gabbronoritic one and an hydrated potassic mafic one) probably occurred penecontemporaneously beneath southern Norway (Vander Auwera et al., 2001). These two distinct sources may reflect increasing degree of metamorphism (amphibolite to granulite) from East to West (Bingen and van Breemen, 1998a) if the gabbronoritic source is a granulite. It could also point to an horizontal stratification of the lower crust (Rudnick and Fountain, 1995), a stratification of the lithosphere (melting of the lower crust or upper mantle) or may indicate that the AMC and granitoid suites belong to two distinct crustal segments as proposed by Duchesne et al. (1999).

Demaiffe et al. (1990) and Demaiffe et al. (1986) indicated that isotopic data on jotunites (AMC suite) and gabbronorites (HBG suite) suggest slightly depleted upper-mantle origin or an origin in the lower crust by melting of depleted mantle-derived basic rocks, shortly (<200 Ma) after their formation. Isotopic data corroborate phase equilibria and bring the additional constraint that, in the case of a partial melting process, emplacement of the basic protolith in

the lower crust must have occurred at an age younger than about 1130 Ma. It is worth emphasizing that a significant magmatic event occurred at 1050 Ma in southern Norway with the emplacement of the calc-alkaline augen gneisses series (Bingen et al., 1993; Bingen and van Breemen, 1998b). The geochemical evolution of these augen gneisses can be accounted for by fractional crystallization of a parent magma resulting from mixing between ultrapotassic, mantle-derived mafic magma (20–25%) with a granodioritic magma generated in the lower crust presumably in a subduction-related geodynamic regime (Bingen et al., 1993). Emplacement of ultrapotassic basalts in the lower crust may thus have occurred around 1050 Ma yielding a plausible protolith for the gabbroic parent magmas of the HBG suite.

The production of large volumes of magmas during a small period of time implies that a major thermal pulse occurred at that time in southern Norway and was likely linked to an important geodynamic feature of the Sveconorwegian evolution. A similar suggestion was proposed by Bingen and van Breemen (1998a) who pointed out that the M2 low-pressure thermal metamorphism dated at 930–925 Ma had a "much broader significance than a local phase of contact metamorphism associated with the intrusion of anorthosite plutons" (p. 351). Similarly, in southwestern USA, the 1.4 Ga A-type magmatism is associated with a broad thermal anomaly (Frost et al., 1999) of regional extension and these authors suggested that the necessary heat was probably supplied by the mantle. The vector of this mantle heat was more likely a linear uprise of the asthenosphere following a lithospheric delamination rather than a mantle plume in intracontinental setting (Albarède, 1998; Frost et al., 2001). Indeed, the HBG suite is roughly linear along the Mandal-Ustaoset shear zone and deep seismic profiles have shown that this shear zone corresponds to a significant Moho offset demonstrating its lithospheric scale (Andersson et al., 1996; Duchesne et al., 1999). Moreover, a plume geodynamic setting has not been favored for AMC suites (Ashwal, 1993). This asthenosphere uprise could be at the origin of the melting of both the hydrated potassic mafic source for HBG generation and the lower crustal gabbronoritic source for AMC generation. Such a geodynamical environment is typical during the postcollisional period (Liégeois et al., 1998).

10. Conclusions

A suite of granitoids, the HBG suite, related to the MUL belongs to the dictinctive group of Proterozoic ferro-potassic A-type granites, also recognized in many cratonic areas and usually defined as "anorogenic". This suite displays an extensive differentiation trend ranging from gabbronorites (50 wt.% SiO_2) to granites (77 wt.% SiO_2) which most probably results from fractional crystallization of several batches of parent basaltic magmas with similar major and trace elements compositions. Moreover, contrarily to what was currently admitted for A-type granites (Loiselle and Wones, 1979), the HBG suite is characterized by relatively high water contents and oxygen fugacity (NNO).

The HBG suite is probably penecontemporaneous with the AMC suite of Rogaland and the parent magmas of these two suites resulted from the partial melting of two different sources: a lower crustal anhydrous, gabbronoritic source for AMC and an hydrous, undepleted to slightly depleted potassic mafic source for the HBG. The penecontemporaneous melting of these two contrasting sources, anhydrous mafic lower crust versus hydrous mafic–ultramafic potassic crust or mantle could reflect increasing degree of metamorphism from East to West, stratification of the lithosphere (mantle versus crust) or of the continental crust itself (Rudnick and Fountain, 1995) or may indicate that the two suites belong to two distinct lithospheric segments as formerly proposed by Duchesne et al. (1999). Linear lithospheric delamination along a major shear zone with consequent asthenospheric uprise could explain the HBG alignment within the MUL.

Acknowledgements

G. Bologne and G. Delhaze are greatly thanked for their analytical and samples preparation work, respectively. I. Roelandts provided F analyses for a selection of samples. Part of the trace element analyses were performed by INAA at Pierre Süe Labaratory, CEN, Saclay, under the supervision of J.-L. Joron, by E.W. who has benefited from an EC doctoral grant at the University of Paris VI. XRF analyses and ICP-MS analyses were performed at the "Collectif

Interinstitutionnel de Géochimie Instrumentale" (University of Liège). Isotopic analyses were performed at the "Centre Belge de Géochronologie" (University of Brussels and Africa Museum, Tervuren). This work was funded by the Belgian Fund for Joint Research. R.F. Emslie and S. Fourcade are greatly acknowledged for their constructive reviews.

References

Albarède, F., 1998. The growth of continental crust. Tectonophysics 296, 1–14.

Allègre, C.J., Treuil, M., Minster, J.-F., Minster, B., Albarède, F., 1977. Systematic use of trace elements in igneous processes. I. Fractional crystallization processes in volcanic suites. Contrib. Miner. Petrology 60, 57–75.

Anders, E., Grevesse, N., 1989. Abundances of the elements: meteoritic and solar. Geochim. Cosmochim. Acta 53, 197–214.

Anderson, J.L., 1987. Proterozoic anorogenic granites of the southwestern United States. In: Jenney, J.P., Reynolds, S.J. (Eds.), Geological Evolution of Arizona, vol. 17. Arizona Geological Digest, pp. 1–26.

Anderson, J.L., 1996. Status of thermobarometry in granitic batholiths. Transactions of the Royal Society of Edinburgh. Earth Sci. 87, 125–138.

Andersen, T., 1997. Radiogenic isotope systematics of the Herefoss granite south Norway: an indicator of Sveconorwegian (Grenvillian) crustal evolution in the Baltic shield. Chem. Geol. 135, 139–158.

Anderson, J.L., Smith, D.R., 1995. The effect of temperature and oxygen fugacity on Al-in-hornblende barometry. Am. Miner. 80, 549–559.

Andersen, T., Maijer, C., Verschure, R.H., 1995. Metamorphism, provenance ages and source characteristics of Precambrian clastic metasediments in the Bamble sector, south Norway. Petrology 3, 321–339.

Andersson, M., Lie, J.E., Husebye, E.S., 1996. Tectonic setting of postorogenic granites within SW Fennoscandia based on deep seismic and gravity data. Terra Nova 8, 558–566.

Andersen, T., Andresen, A., Sylvester, A.G., 2001. Nature and distribution of deep crustal reservoirs in the southwestern part of the Baltic shield: evidence from Nd, Sr and Pb isotope data on late Sveconorwegian granites. J. Geol. Soc. Lond. 158, 253–267.

Ashwal, L., 1993. Anorthosites. Springer-Verlag, New York, p. 422.

Bau, M., 1996. Controls on the fractionation of isovalent trace elements in magmatic and aqueous systems: evidence from Y/Ho, Zr/Hf, and lanthanide tetrad effect. Contrib. Miner. Petrology 123, 323–333.

Bingen, B., van Breemen, O., 1998a. U-Pb monazite ages in amphibolite- to granulite-facies orthogneiss reflect hydrous mineral breakdown reactions: Sveconorwegian Province of SW Norway. Contrib. Miner. Petrology 132, 336–353.

Bingen, B., van Breemen, O., 1998b. Tectonic regimes and terrane boundaries in the high-grade Sveconorwegian belt of SW Norway, inferred from U-Pb zircon geochronology and geochemical signature of augen gneisses suites. J. Geol. Soc. Lond. 155, 143–154.

Bingen, B., Demaiffe, D., Hertogen, J., Weis, D., Michot, J., 1993. K-rich calc-alkaline augen gneisses of Grenvillian age in SW Norway: mingling of mantle-derived and crustal components. J. Geol. 101, 763–778.

Bingen, B., Birkeland, A., Nordgulen, O., Sigmond, E., 2001. Correlation of supracrustal sequences and origin of terranes in the Sveconorwegian orogen of SW Scandinavia: SIMS data on zircon in clastic sediments. Precambrian Res. 108, 293–318.

Bogaerts, M., Scaillet, B., Liégeois, J.-P., Vander Auwera, J., 2003. Petrology of the Lyngdal granodiorite (southern Norway) and the role of fractional crystallization in the genesis of Proterozoic rapakivi-like granites. Precambrian Res. 124, 149–184.

Bogaerts, M., Scaillet, B., Vander Auwera, J., 2001. Experimental determination of the Lyngdal granodiorite (southern Norway). J. Conf. Abs. 6, 770.

Bolle, O., Diot, H., Trindade, R., in press. Magnetic fabrics in the Holum granite (Vest-Agder, southernmost Norway): implications for the late evolution of the Sveconorwegian (Grenvillian) orogen of SW Scandinavia. Precambrian Res.

Bologne G., Duchesne, J.C., 1991. Analyse des roches silicatées par spectrométrie de fluorescence X: précision et exactitude. Service Géologique de Belgique, Professional Paper 249(5), 1–11.

Brown, G.C., 1981. Space and time in granite plutonism. Philos. Trans. R. Soc. Lond. A301, 321–336.

Chauvel, C., Blichert-Toft, J., 2001. A hafnium isotope and trace element perspective on melting of the depleted mantle. Earth Planetary Sci. Lett. 190, 137–151.

Clemens, D.J., Holloway, J.R., White, A.J.R., 1986. Origin of an A-type granite: experimental constraints. Am. Miner. 71, 317–324.

Dall'Agnol, R., Scaillet, B., Pichavant, M., 1999. An experimental study of a lower Proterozoic A-type granite from the eastern Amazonian Craton, Brazil. J. Petrology 40, 1673–1698.

Debon, F., Le Fort, P., 1983. A chemical–mineralogical classification of common plutonic rocks and associations. Transactions of the Royal Society of Edinburgh. Earth Sci. 73, 135–149.

Demaiffe, D., Hertogen, J., 1981. Rare earth geochemistry and strontium isotopic composition of a massif-type anorthositic-charnockitic body: the Hidra massif (Rogaland SW Norway). Geochim. Cosmochim. Acta 45, 1545–1561.

Demaiffe, D., Weis, D., Michot, J., Duchesne, J.C., 1986. Isotopic constraints on the genesis of the Rogaland anorthositic suite (southwest Norway). Chem. Geol. 57, 167–179.

Demaiffe, D., Bingen, B., Wertz, P., Hertogen, J., 1990. Geochemistry of the Lyngdal hyperites (SW Norway): comparison with the monzonorites associated with the Rogaland anorthosite complex. Lithos 24, 237–250.

Dons, J.A., 1960. The stratigraphy of supracrustal rocks, granitization and tectonics in the Precambrian Telemark area, southern Norway. Guide to excursion A10. In: Proceedings

of the 21st International Geol Congress, vol. 212. Norges Geologisk Undersokelse, Norden, p. 30.

Droop, G.T.R., 1987. A general equation for estimating Fe^{3+} concentrations in ferromagnesian silicates and oxides from microprobe analyses, using stoichiometric criteria. Miner. Mag. 51, 431–435.

Duchesne, J.C., Wilmart, E., 1997. Igneous charnockites and related rocks from the Bjerkreim-Sokndal layered intrusion (southwest Norway): a jotunite (hypersthene monzodiorite)-derived A-type granitoid suite. J. Petrology 38, 337–369.

Duchesne, J.C., Roelandts, I., Demaiffe, D., Hertogen, J., Gijbels, R., de Winter, J., 1974. Rare-earth data on monzonoritic rocks related to anorthosites and their bearing on the nature of the parental magma of the anorthositic series. Earth Planetary Sci. Lett. 24, 325–335.

Duchesne, J.C., Berza, T., Liégeois, J.-P., Vander Auwera, J., 1998. Shoshonitic liquid line of descent from diorite to granite: the late Precambrian postcollisional Tismana pluton (south Carpathians, Romania). Lithos 45, 281–303.

Duchesne, J., Liégeois, J.-P., Vander Auwera, J., Longhi, J., 1999. The crustal tongue melting model and the origin of massive anorthosites. Terra Nova 11, 100–105.

Eby, G.N., 1990. The A-type granitoids: a review of their occurrence and chemical characteristics and speculations on their petrogenesis. Lithos 26, 115–134.

Emslie, R.F., 1991. Granitoids of rapakivi granite-anorthosite and related associations. Precambrian Res. 51, 173–192.

Emslie, R.F., Stirling, J.A.R., 1993. Rapakivi and related granitoids of the Nain plutonic suite: geochemistry, mineral assemblages and fluid equilibria. Can. Miner. 31, 821–847.

Falkum, T., 1998. The Sveconorwegian magmatic and tectono-metamorphic evolution of the high-grade Proterozoic Flekkefjord complex, south Norway. Norges Geologisk Undersökelse 434, 5–34.

Falkum, T., Petersen, J.S., 1974. A three-fold division of the "farsundite" plutonic complex at Farsund, southern Norway. Norsk Geologisk Tidsskrift 54, 361–366.

Falkum, T., Wilson, J.R., Annis, M.P., Fregerslev, S., Zimmermann, H., 1972. The intrusive granites of the Farsund area, south Norway. Norsk Geologisk Tidsskrift 52, 463–465.

Falkum, T., Wilson, J., Petersen, J., Zimmermann, H.D., 1979. The intrusive granites of the Farsund area, south Norway. Their interrelations and relations with the Precambrian metamorphic envelope. Norsk Geologisk Tidsskrift 59, 125–139.

Frost, C.D., Frost, B.R., 1997. Reduced rapakivi-type granites: the tholeiite connection. Geology 25, 647–650.

Frost, C.D., Frost, B.R., Chamberlain, K.R., Edwards, B.R., 1999. Petrogenesis of the 1.43 Ga Sherman batholith SE Wyoming USA: a reduced rapakivi-type anorogenic granite. J. Petrology 40, 1771–1802.

Fuhrman, M.I., Frost, B.R., Lindsley, D.H., 1988. Crystallization conditions of the Sybille monzosyenite, Laramie Anorthosite Complex, Wyoming. J. Petrology 29, 699–729.

Grove, T.L., Bryan, W.B., 1983. Fractionation of pyroxene-phyric MORB at low pressure: an experimental study. Contrib. Miner. Petrology 84, 293–309.

Hanson, G.N., 1978. The application of trace elements to the petrogenesis of igneous rocks of granitic composition. Earth Planetary Sci. Lett. 38, 26–43.

Harrison, T.M., Watson, E.B., 1984. The behavior of apatite during crustal anatexis: equilibrium and kinetic considerations. Geochim. Cosmochim. Acta 48, 1467–1477.

Holland, T., Blundy, J., 1994. Non-ideal interactions in calcic amphiboles and their bearing on amphibole-plagioclase thermometry. Contrib. Miner. Petrology 116, 443–447.

Irber, W., 1999. The lanthanide tetrad effect and its correlation with K/Rb, Eu/Eu*, Sr/Eu, Y/Ho, and Zr/Hf of evolving peraluminous granite suites. Geochim. Cosmochim. Acta 63, 489–508.

Irvine, T.N., Baragar, W.R.A., 1971. A guide to the chemical classification of the common volcanic rocks. Can. J. Earth Sci. 8, 523–548.

Jacobsen, S.B., Heier, K.S., 1978. Rb-Sr isotope systematics in metamorphic rocks Kongsberg, sector, south Norway. Lithos 11, 257–276.

Jahn, B., Wu, F., Capdevila, R., Martineau, F., Zhao, Z., Wang, Y., 2001. Highly evolved juvenile granites with tetrad REE patterns: the Woduhe and Baerzhe granites from the Great Xing'an Mountains in NE China. Lithos 59, 171–198.

Johnson, M.C., Rutherford, M.J., 1989. Experimental calibration of the aluminium-in-hornblende geobarometer with application to Long Valley caldera (California) volcanic rocks. Geology 17, 837–841.

Killeen, P.G., Heier, K.S., 1975. Th, U, K, and heat production measurements in ten Precambrian granites of the Telemark area, Norway. Norges Geologisk Undersokelse 319, 59–83.

Kolker, A., Lindsley, D.H., 1989. Geochemical evolution of the Maloin Ranch pluton, Laramie Anorthosite Complex, Wyoming: petrology and mixing relations. Am. Miner. 74, 307–324.

Leake, B., 1978. Nomenclature of amphiboles. Can. Miner. 16, 501–520.

Liégeois, J.-P., 1988. Le batholite composite de l'Adrar des Iforas (Mali). Académie royale des Sciences d'Outre-mer, Classe des Sciences Naturelles et Médicales, p. 231.

Liégeois, J.-P., Black, R., 1987. Alkaline magmatism subsequent to collision in the Pan-African belt of the Adrar des Iforas. In: Fitton, J.G., Upton, B.G.J. (Eds.), Alkaline Igneous Rocks. The Geological Society, Blackwell, pp. 381–401.

Liégeois, J.-P., Navez, J., Hertogen, J., Black, R., 1998. Contrasting origin of postcollisional high-K calc-alkaline and shoshonitic versus alkaline and peralkaline granitoids. The use of sliding normalization. Lithos 45, 1–28.

Loiselle, M.C., Wones, D., 1979. Characteristics and origin of anorogenic granites. Geol. Soc. Am. Abs. Prog. 11, 468.

Longhi, J., Vander Auwera, J., Fram, M., Duchesne, J.C., 1999. Some phase equilibrium constraints on the origin of Proterozoic massif anorthosites and related rocks. J. Petrology 40, 339–362.

Ludwig, K.R., 2001. User's Manual for Isoplot/Ex Version 2.49: A Geochronological Toolkit for Micrososft EXCEL. Berkeley Geochronology Center, Special Publication, 1a.

Mahood, G., Hildreth, W., 1983. Large partition coefficients for trace elements in high-silica rhyolites. Geochim. Cosmochim. Acta 47, 11–30.

Menuge, J., 1982. Nd isotope studies of crust-mantle evolution: the Proterozoic of south Norway and the Archean of south Africa. Ph.D. thesis, Cambridge University, United Kingdom.

Menuge, J., 1988. The petrogenesis of massif anorthosites: a Nd and Sr isotopic investigation of the Proterozoic of Rogaland/Vest-Agder, SW Norway. Contrib. Miner. Petrology 98, 363–373.

Mitchell, J.N., Scoates, J., Frost, C.D., 1995. High-Al gabbros in the Laramie Anorthosite Complex, Wyoming: implications for the composition of melts parental to Proterozoic anorthosite. Contrib. Miner. Petrology 119, 166–180.

Nelson, B.K., DePaolo, D.J., 1984. 1700 Myr greenstone volcanic successions in southwestern North America and isotopic evolution of Proterozoic mantle. Nature 312, 143–146.

Pasteels, P., Michot, J., 1975. Geochronological investigation of the metamorphic terrain of southwestern Norway. Norsk Geologisk Tidsskrift 55, 111–134.

Pasteels, P., Demaiffe, D., Michot, J., 1979. U-Pb and Rb-Sr geochronology of the eastern part of the south Rogaland igneous complex, southern Norway. Lithos 12, 199–208.

Peccerillo, A., Taylor, S.R., 1976. Geochemistry of eocene calc-alkaline volcanic rocks from the Kastamonu area northern Turkey. Contrib. Miner. Petrology 58, 63–81.

Perchuk, L.L., Aranovich, L.Y., Podlesskii, K.K., Lavrant'eva, I.V., Gerasimov, V.Y., Fed'kin, V.V., Kitsul, V.I., Karsakov, L.P., Berdnikov, N.V., 1985. Precambrian granulites of the Aldan shield eastern Siberia, USSR. J. Metamorphic Geol. 3, 265–310.

Petersen, J.S., 1980a. Rare-earth element fractionation and petrogenetic modelling in charnockitic rocks SW Norway. Contrib. Miner. Petrology 73, 161–172.

Petersen, J.S., 1980b. The zoned Kleivan granite: an end-member of the anorthositic suite in SW Norway. Lithos 13, 79–95.

Poitrasson, F., Duthou, J.L., Pin, C., 1995. The relationship between petrology and Nd isotopes as evidence for contrasting anorogenic granite genesis: example of the Corsican Province (SE France). J. Petrology 36, 1251–1274.

Priem, H., Verschure, R., 1982. Review of the isotope geochronology of the high-grade metamorphic Precambrian of SW Norway. Geologische Rundschau 71, 81–84.

Rapp, R.P., Watson, E.B., 1995. Dehydration melting of metabasalt at 8–32 kbar: implications for continental growth and crust-mantle recycling. J. Petrology 36, 891–931.

Rickwood, P.C., 1989. Boundary lines within petrologic diagrams which use oxides of major and minor elements. Lithos 22, 247–264.

Roelandts, I., Robaye, G., Weber, G., Delbrouck, J.M., Duchesne, J.C., 1987. Determination of fluorine by proton-induced gamma-ray emission (PIGE) spectrometry in igneous and metamorphic charnockitic rocks from Rogaland (SW Norway). J. Radionuclear Chem. 112, 453–460.

Rudnick, R.L., Fountain, D.M., 1995. Nature and composition of the continental crust: a lower crustal perspective. Rev. Geophys. 33, 267–309.

Schärer, U., Wilmart, E., Duchesne, J.C., 1996. The short duration and anorogenic character of anorthosite magmatism: U-Pb dating in the Rogaland complex, Norway. Earth Planetary Sci. Lett. 139, 335–350.

Schmidt, M., 1992. Amphibole composition in tonalite as a function of pressure: an experimental calibration of the Al-in-hornblende. Contrib. Miner. Petrology 110, 304–310.

Sigmond, E.M.O., 1985. The Mandal-Ustaoset Line, a newly discovered major fault zone in south Norway. In: Tobi, A., Touret, J. (Eds.), The Deep Proterozoic Crust in the North Atlantic Provinces. NATO Advanced Study Institute Series Reidel, Dordrecht, pp. 323–331.

Steiger, R.H., Jäger, E., 1977. Subcommission on geochronology: convention on the use of decay constants in geo- and cosmochronology. Earth Planetary Sci. Lett. 36, 359–362.

Streckeisen, A.L., 1976. To each plutonic rock its proper name. Earth Sci. Rev. 12, 1–33.

Sun, S.S., Mc Donough, W.F., 1989. Chemical and isotopic systematics of oceanic basalts: implications for mantle composition and processes. In: Saunders, A., Norry, M. (Eds.), Magmatism in the Ocean Basins. Geological Society Special Publication, Blackwell, pp. 313–345.

Sylvester, A.G., 1998. Magma mixing, structure, and re-evaluation of the emplacement mechanism of the Vradal pluton, central Telemark, southern Norway. Norsk Geologisk Tidsskrift 78, 259–276.

Tobi, A., Hermans, G., Maijer, C., Jansen, J., 1985. Metamorphic zoning in the high-grade Proterozoic of Rogaland-Vest Agder, SW Norway. In: Tobi, A.T., J.L.R. (Eds.), The Deep Proterozoic Crust in the North Atlantic Provinces. NATO Advanced Study Institute Series, Reidel, Dordrecht, pp. 477–497.

Turner, S.P., Foden, J.D., Morrisson, R.S., 1992. Derivation of some A-type magmas by fractionation of basaltic magma: an example of the Pathway Ridge, south Australia. Lithos 28, 151–179.

Vander Auwera, J., Longhi, J., 1994. Experimental study of a jotunite (hypersthene monzodiorite): constraints on the parent magma composition and crystallization conditions (P, T, fO2) of the Bjerkreim-Sokndal layered intrusion (Norway). Contrib. Miner. Petrology 118, 60–78.

Vander Auwera, J., Longhi, J., Duchesne, J.C., 1998a. A liquid line of descent of the jotunite (hypersthene monzodiorite) suite. J. Petrology 39, 439–468.

Vander Auwera, J., Bologne, G., Roelandts, I., Duchesne, J.C., 1998b. Inductively coupled plasma-mass spectrometric (ICP-MS) analysis of silicate rocks and minerals. Geol. Belgica 1, 49–53.

Vander Auwera, J., Liégeois, J.-P., Demaiffe, D., Bolle, O., Bogaerts, M., Duchesne, J.C., 2001. Two distinct postcollisional magmatic suites in the Sveconorwegian of southern Norway: consequence for the evolution of the Proterozoic continental lithosphere. J. Conf. Abs. 6, 769.

Watson, E.M., Harrison, T.M., 1983. Zircon saturation revisited: temperature and compositional effects in a variety of crustal magma types. Earth Planetary Sci. Lett. 64, 295–304.

Whalen, J.B., Currie, K.L., Chappell, B.W., 1987. A-type granites: geochemical characteristics discrimination and petrogenesis. Contrib. Miner. Petrology 95, 407–419.

Wielens, J.B.W., Andriessen, P.A.M., Boelrijk, N.A.M., Hebeda, E.H., Priem, H.N.A., Verdumen, E.A.T., Verschure, R.H., 1981. Isotope geochronology in the high-grade metamorphic Precam-

brian of southwestern Norway: new data and reinterpretations. Norges Geologisk Undersokelse Bull. 359, 1–30.

Wilmart, E., Demaiffe, D., Duchesne, J.C., 1989. Geochemical constraints on the genesis of the Tellnes ilmenite deposit, southwest Norway. Econ. Geol. 84, 1047–1056.

Wilson, J.R., Robins, B., Nielsen, F.M., Duchesne, J.C., Vander Auwera, J., 1996. The Bjerkreim-Sokndal layered intrusion, southwest Norway. In: Cawthorn, R.G. (Ed.), Layered Intrusions. Elsevier, Amsterdam, pp. 231–255.

Wilson, J.R., Pedersen, S., Berthelsen, C.R., Jakobsen, B.M., 1977. New light on the Precambrian Holum granite. Norsk Geologisk Tidsskrift 57, 347–360.

Wones, D.R., 1989. Significance of the assemblage titanite + magnetite + quartz in granitic rocks. Am. Miner. 74, 744–749.

Zhou, X., Bingen, B., Demaiffe, D., Liégeois, J.-P., Hertogen, J., Weis, D., Michot, J., 1995. The 1160 Ma Hidderskog meta-charnockite: implications of this A-type pluton for the Sveconorwegian belt in Vest Agder (SW Norway). Lithos 36, 51–66.